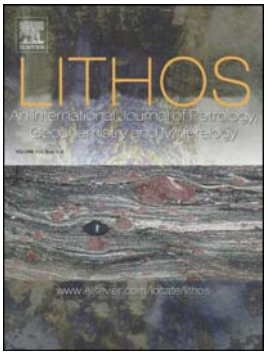

Origin and age of zircon-bearing chromitite layers from the Finero Phlogopite Peridotite (Ivrea-Verbano Zone, western Alps) and geodynamic consequences

Alberto Zanetti, Tommaso Giovanardi, Antonio Langone, Massimo Tiepolo, Fu-Yuan Wu, Luigi Dallai, Maurizio Mazzucchelli

PII: S0024-4937(16)30128-1
DOI: doi: 10.1016/j.lithos.2016.06.015
Reference: LITHOS 3961

To appear in: *LITHOS*

Received date: 3 December 2015
Accepted date: 17 June 2016

Please cite this article as: Zanetti, Alberto, Giovanardi, Tommaso, Langone, Antonio, Tiepolo, Massimo, Wu, Fu-Yuan, Dallai, Luigi, Mazzucchelli, Maurizio, Origin and age of zircon-bearing chromitite layers from the Finero Phlogopite Peridotite (Ivrea-Verbano Zone, western Alps) and geodynamic consequences, *LITHOS* (2016), doi: 10.1016/j.lithos.2016.06.015

Origin and age of zircon-bearing chromitite layers from the Finero Phologopite Peridotite (Ivrea-Verbano Zone, western Alps) and geodynamic consequences

Alberto Zanetti[1], Tommaso Giovanardi[2], Antonio Langone[1], Massimo Tiepolo[3], Fu-Yuan Wu[4], Luigi Dallai[5], Maurizio Mazzucchelli[6,1].

1Istituto di Geoscienze e Georisorse - CNR, Unità di Pavia, Via Ferrata, 1, I-27100 Pavia, Italy;
2Instituto de Geociências, Universidade de São Paulo, Rua do Lago, 562, Cidade Universitária, 05508-900 São Paulo, Brazil;
3Dipartimento di Scienze della Terra 'Ardito Desio', Università degli Studi di Milano, Via Mangiagalli/Botticelli, 32/23, I-20133 Milano, Italy;
4State Key Laboratory of Lithospheric Evolution, Institute of Geology and Geophysics, Chinese Academy of Sciences, P. O. Box 9825, 100029 Beijing, China;
5Istituto di Geoscienze e Georisorse - CNR, Sede di Pisa, Via Giuseppe Moruzzi, 1, I-56124 Pisa, Italy;
6Dipartimento di Scienze Chimiche e Geologiche, Università di Modena e Reggio Emilia, Via Campi, 103, I-41125 Modena, Italy.

Corresponding Author: Tommaso Giovanardi; e-mail: tommaso.giovanardi@gmail.com

Abstract

An investigation has been performed on three chromitite layers segregated in dunite bodies of the Phlogopite Peridotite mantle unit in the Finero Complex (FPP, Ivrea–Verbano Zone, Southern Alps) aimed at providing new constraints to their origin and evolution.

Field relationships, the sub-chondritic Hf isotopic composition of the zircons ($\varepsilon Hf_{(188)}$ as low as -5.4), the heavy O isotopic composition of zircons and pyroxenes ($\delta^{18}O$ up to 6.9‰), the strict similarity of the trace element composition between the clinopyroxenes and amphiboles from the

chromitites and those from the phlogopite harzburgites and pyroxenites forming the typical FPP association, as well as the REE composition of zircons, which approaches equilibrium with the associate clinopyroxene, suggest that the studied chromitites were segregated from melts, highly contaminated from continental crust, during the pervasive cycle of metasomatism recorded by the FPP. A LA-ICP-HRMS survey of chromitite zircon grains has provided Early Jurassic U-Pb ages mostly between 199 ± 3 Ma and 178 ± 2 Ma, with a pronounced peak at 187 Ma. Relevant exceptions are inherited domains of two grains giving Triassic ages of 242 ± 7 Ma and 229 ± 7 Ma, and a third homogeneous zircon giving 208 ± 3 Ma. Our geochronological data and those reported in the literature show that the FPP chromitites have zircon populations with different internal CL textures, but the same sub-chondritic Hf isotopic composition, which define an overall U-Pb age span from ~290 Ma to 180. The segregation of the chromitite layers and the main pervasive metasomatism likely occurred in the Early Permian (in a post-collisional, transtensional setting) or before (possibly, in a subduction-related setting). The rejuvenation of the zircon ages was accompanied by a progressive disapperance of the internal zoning, interpreted as the result of a prolonged residence at mantle depths with progressive re-equilibration of the U-Pb system due to thermal perturbations. The age peak at ~187 Ma is argued to constrain the timing of FPP exhumation at shallower, crustal levels. This process was characterised by an important reheating event, possibly due to lithospheric hyperextension. The evolution of the FPP appears completely different than that of mantle bodies of the central IVZ (i.e. the Val Sesia-Type bodies), which were emplaced within the continental crust, as part of accretionary prisms, at or before the end of the Variscan orogeny.

Keywords: Finero; zircon; mantle; chromitite; metasomatism.

Introduction

The Ivrea-Verbano Zone (IVZ, Southern Alps, Italy-Switzerland) consists of a worldwide famous section of lower continental crust. The reference geodynamic model developed after detailed field, geochronological and geochemical investigation of its central part (i.e. Sesia and Sessera Valleys) involves Early Permian under- and intra-plating of mafic melts, which interacted with granulite to amphibolite-facies metamorphic basement and evolved towards acid compositions producing granite intrusions and rhyolite volcanism (Quick et al., 1995, 2009; Sinigoi et al., 1996, 2011; Mazzucchelli et al., 2014).

Zanetti et al. (2013, 2014) pointed out that the northern sector of the IVZ records a number of structural, petrochemical and age anomalies with respect to such a model. For instance, there is now abundant evidence of the occurrence in the Finero Mafic Complex (northernmost IVZ) of widespread events of Triassic magmatism (Gebauer, 1993; Lu et al., 1997a,b; Hingerl et al., 2008; Zanetti et al., 2013, 2014; Klötzli, Personal Communication), with late alkaline veins and pockets (e.g. zircon-bearing diorites and nepheline diorite pegmatites) mostly showing Late Triassic to Early Jurassic ages (Oppizzi and Schaltegger, 1999; Grieco et al., 2001; Klötzli et al., 2007, 2009; Schaltegger et al., 2015, and references therein). Late Triassic intrusions of zircon-bearing diorites, associated to hornblendites (Stähle et al., 1990, 2001; Grieco et al., 2001), are also recorded by the associate mantle unit, the Finero Phlogopite Peridotite (FPP), which also shows peculiar late, discordant swarms of apatite-calcite-bearing gabbroic veins characterised by the presence of magmatic sapphirine (Giovanardi et al., 2013). A 225 Ma age has been found in a recrystallised rim of a zircon from a metasedimentary septum included in the intrusive External Gabbro unit and in a monazite from the adjacent Kinzigite Formation (Langone and Tiepolo, 2015).

These observations suggest the occurrence of two kinds of IVZ, the “Val Sesia”-Type (central IVZ) and the “Finero”-Type (northern IVZ), assumed to have had different tectono-magmatic evolutions (Rivalenti and Mazzucchelli, 2000; Zanetti et al., 2013, 2014; Mazzucchelli et al., 2014). Further main differences are the petrochemical features of the mantle bodies. The Val Sesia-Type mantle bodies are constituted by refractory spinel peridotites, virtually free from metasomatism away from

pyroxenites and dunite channels (Rivalenti et al., 1981, 1995; Mazzucchelli et al., 2009). Conversely, the Finero-Type mantle bodies are enriched in phlogopite and amphibole due to diffuse modal metasomatism (Rivalenti and Mazzucchelli, 2000; Zanetti et al., 2013; Mazzucchelli et al., 2014). According to the distribution of the different kinds of mantle peridotites, Zanetti et al. (2013) have speculatively proposed that their boundary may corresponds to the Anzola-Val Grande high temperature shear zone (HTSM in Fig. 1).

The FPP is the biggest mantle body of the northern IVZ. It shows a virtually complete recrystallization due to pervasive to channelled melt migrations (Zanetti et al., 1999). The pervasive metasomatism formed a main lithologic association constituted by phlogopite harzburgites associated to phlogopite pyroxenites (mainly websterites and orthopyroxenites), which do not show significant chemical gradients among them (Zanetti et al., 1999). The channelled migration stages formed dunite bodies, often containing stratiform to podiform chromites and, more rarely, pyroxenite and hornblendite layers (Cumming et al., 1987; Hartmann and Wedepohl, 1993; Zanetti et al., 1999; Seitz and Woodland, 2000; Grieco et al., 2001, 2004; Zaccarini et al., 2004; Raffone et al., 2006; Selverstone and Sharp, 2011; Giovanardi, 2012; Mazzucchelli et al., 2014). Relatively late melt migration events also formed peridotite and pyroxenite veins and bands (Zanetti et al., 1999, Grieco et al., 2001; Morishita et al., 2003, 2008; Matsumoto et al. 2005; Raffone et al., 2006). These are often characterised by the presence of apatite and carbonates, and usually exhibit marked modal and chemical gradients with respect to the host phlogopite harzburgite. Examples of these lithologies are the apatite-dolomite-bearing wehrlites (Zanetti et al., 1999; Raffone et al., 2006), as well as the apatite-bearing orthopyroxenites described by Morishita et al. (2003, 2008), and Matsumoto et al. (2005), these latter displaying Triassic ages.

Thanks to such a unique lithological association, the FPP is one of the most studied mantle sequence in the world (Fig. 1). Several papers have dealt with the age of the petrochemical processes and the geochemical affinity of the melts that migrated through it. These melts only marginally match the magmatic record of the associated crustal rocks of the Finero Mafic Complex

(Giovanardi et al., 2014). Despite this, the geodynamic evolution of the FPP is still controversial and the geochemical affinity of the metasomatic melts strongly debated. In particular, geochronological surveys reported in the literature give a very large age interval, spanning from the Early Permian to the Early Jurassic, which is difficult to reconcile with the evidence that the mantle bodies of the central IVZ (i.e. the Balmuccia body) were emplaced within the continental crust, as part of accretionary prisms, at or before the end of the Variscan orogeny.

A special opportunity to place geochronological constraints on the evolution of the FPP is represented by the occurrence of large amounts of primary zircon in the chromitites (Ferrario and Garuti, 1990; Grieco et al., 2001; Zaccarini et al., 2004). Thus, three chromitite swarms segregated in dunite bodies of the FPP were investigated. Zircon and associate minerals have been subjected to a detailed petrochemical investigation in order to shed light on i) the geochemical affinity of their parent melts, ii) the age of the metasomatism and iii) the geodynamic evolution of the mantle sequences in the Finero-Type IVZ.

Geological setting and selected samples

The IVZ represents the westernmost sector of the Southern Alps, which form the inner part of the Alpine orogen. The Southern Alps escaped Alpine subduction, thus preserving their lithospheric mantle roots. In the IVZ, the lithologies were tilted about of 90° at the end of the Middle Miocene (Wolff et al., 2012), as a consequence of a series of rotations started with the opening of the Jurassic Tethys and culminated with the Alpine collision and relaxation of the Alpine orogen (Rutter et al., 2007; Wolff et al., 2012; Beltrando et al., 2015). The Finero Complex outcrops as an antiform in the northernmost part of IVZ. The antiform core is composed by the Finero Phlogopite Peridotite mantle unit (FPP; Cawthorn, 1975), which is wrapped by an intercalation of mafic-ultramafic lithologies interpreted as pristine intrusive bodies (Cawthorn, 1975; Coltorti and Siena, 1984; Lu et al., 1997a, b), and referred to as the Finero Mafic Complex (Fig. 1). The latter consists (from the contact with the FPP outwards) of: i) the Layered Internal Zone (LIZ), ii) the Amphibole Peridotite

(AP) and iii) the External Gabbro (EG). To the N-NW, the Finero Complex is in contact across the Insubric line with an accretionary prism of the Alpine orogeny, namely the Sesia-Lanzo Zone, belonging to the Austroalpine domain (Fig. 1). To the S-SE, it is instead bounded by the metapelites and metavolcanics, from granulite-to-amphibolite-facies, of the Kinzigite Formation, i.e. the polymetamorphic basement of the Adria plate (Fig. 1).

In the FPP, stratiform to podiform chromitites mainly occur in dunite bodies. The petrogenesis of the FPP chromitites has previously been discussed by Ferrario and Garuti (1990), Garuti et al. (1997), Grieco et al. (2001, 2004) and Zaccarini et al. (2004), with the peculiar presence of zircons being firstly recognised by Ferrario and Garuti (1990). The chromitites locally contain abundant Fe-Ni-Cu-sulphides and Platinum Group Elements (PGE) minerals, but also zirconolite, baddeleyite, thorianite, uraninite, thorite or huttonite (Grieco et al., 2004; Zaccarini et al., 2004).

The dunite bodies were produced by stages of channelled melt migration (Grieco et al., 2001, 2004; Zaccarini et al., 2004). Most of them are elongated parallel to the mantle foliation and show sharp contacts with the host phlogopite-harzburgite and pyroxenite association. The abrupt change of the mineralogy is apparently the result of tectonic reactivation of the lithologic discontinuity. However, some gradational transitions between dunites and host harzburgites are preserved (Zaccarini et al., 2004). In particular, a gradational transition has been observed for peculiar dunite bodies having elongations highly discordant to the mantle foliation (Giovanardi, 2012).

Field observations indicate that large concordant dunites (up to 20 m across) i) may be virtually free from late magmatic segregations or layers; ii) contain chromitite layers (from a few mm to dm); iii) possess chromitites layers associate to the late intrusion of magmatic sheets, (Giovanardi, 2012). Field relationships indicate that the chromitite segregation preceded formation of the other magmatic layers inside the dunite bodies, consistent with the observation reported by Grieco et al. (2001, 2004).

The chromitite swarms here studied formed in dunite bodies outcropping in different sectors of the FPP unit. At outcrop scale, no late phlogopite-amphibole-bearing magmatic layers are associated to

these chromitites. The samples selected are representative of two different chromitite end-members (Fig. 2). In particular, one sample (MR01CR) records only a large segregation of chromite with modest recovery of the previous texture dominated by deformed dunite olivine (hereafter Ol-chromitite; where Ol means olivine, Fig. 2c), while two samples document the complete recovery of the dunite texture, which is totally replaced by secondary chromite and orthopyroxene (hereafter Opx-chromitite, where Opx means orthopyroxene). The Ol-chromitite swarm, consisting of 1-cm thick parallel layers, outcrops in the area of Mount Sasso Rosso (MR01CR; Fig. 1). The chromitite layers are made of large, anhedral, locally round chromite grains crystallised in a strongly-deformed porphyroclastic dunite characterised by the presence of olivine porphyroclasts embedded in a fine-grained matrix. The latter basically consists of olivine, with subordinate, anhedral orthopyroxene, in part clearly overgrowing olivine. Very small clinopyroxene and amphibole grains have been detected by SEM-EDS inspection, while phlogopite is missing. Thorite was recognized during SEM-EDS inspection (Supplementary Material C). The two Opx-chromitites (FI09C04 and FI09C34; Fig. 2a, b) outcrop along the Cannobino river to the south of Finero, close to the bridge towards Provola (Fig. 1). The single chromitite layers of the Cannobino occurrences, up to 6 cm in thickness, locally merge in pockets up to 20 cm large (Fig. 2b). These chromitites show allotriomorphic texture and are mainly composed by chromite and orthopyroxene (chromite 75-55% by Vol.; orthopyroxene 35-15% by Vol.: Fig. 2d, e), with subordinate clinopyroxene, apparently in textural equilibrium with the other minerals. In these samples, olivine rarely occurs as very small, round relicts embedded in large orthopyroxenes. Phlogopite is missing, whereas rare amphibole grains, few tens of μm large, have been detected by SEM-EDS inspection. An Opx-chromitite sample with similar modal composition to those here studied was documented by Grieco et al. (2004).

According to Ferrario and Garuti (1990), Grieco et al. (2001) and Zaccarini et al. (2004), zircons are up to 600 μm long. Euhedral zircons occur within chromite and sometimes in olivine. Most

frequently, they are anhedral to subhedral, in interstitial position between chromite and olivine and/or orthopyroxene. Up to 25 zircons were observed in 50 mm^2 by Zaccarini et al. (2004).

Analytical methods

Separation of orthopyroxene, clinopyroxene and zircon was performed with magnetic and chromatographic methods at the IGG-CNR, Pisa. The rocks were first grinded in two different granulometries: 0.250 to 0.125 mm and less than 0.125 mm. Minerals were then concentrated and purified by hand picking under a binocular microscope. Sixty-one zircons were separated from MR01CR, 11 from FI09C34 and 54 from FI09C04 and mounted in resin. Zircon internal structure was characterized with cathode-luminescence (CL) imaging by means of a SEM (Jeol JXA 840A model) at IGG-CNR, Pavia. Geochronological data were obtained with ELA-ICP-HRMS at the IGG-CNR, Pavia. The instrument couples an ArF excimer laser microprobe of 193 nm (Geolas200Q-Microlas) with a ThermoFinnigan Element I ICP-HRMS. Mass signals 202 (Hg), 204 (Pb + Hg), 206 (Pb), 207 (Pb), 208 (Pb), 232 (Th) and 238 (U) were acquired in magnetic scan mode (Tiepolo, 2003). The laser was operated at a repetition rate of 5 Hz with a pulse-energy of about 12 J/cm^2; Instrumental and laser-induced U/Pb fractionations were simultaneously corrected using as external standard the 1065 Ma 91500 reference zircon (Widenbeck et al., 1995). The same integration intervals and spot size were used on both the external standard and unknowns. During each analytical run reference zircon 02123 (295 Ma; Ketchum et al., 2001) was analysed together with unknowns for quality control, accuracy resulted better than 99%. The spot size was set to 20 mm and laser fluency to 12J/cm^2. Data reduction was carried out using the "Glitter" software package (van Achterbergh et al., 2001) setting at 1% the error of the external standard. During each analytical run the reproducibility on the standards was propagated to all determinations according to the equation in Horstwood et al. (2003). After this operation, analyses are considered accurate within quoted errors. . All the analyses in the present work yield count rates for ^{204}Pb at background level therefore no common Pb correction was carried out. The reader would however consider that

the relatively high background of Hg hampers the detection of low signals for ^{204}Pb. Ages were calculated for $^{207}Pb/^{206}Pb$, $^{206}Pb/^{238}U$ and $^{207}Pb/^{235}U$ ratios with 2σ error (Tab. 1) using Isoplot software (Ludwig, 2003). Concordia ages were determined and concordia plots were constructed using the same software. All errors in the text are given at 2s level.

Mineral major element analyses were conducted with the electron microprobe JEOL 8200 Super Probe housed at the University of Milano (data are reported in Supplementary Material Tab. A) on petrographic sections after carbon coating. Analytical conditions were 15 kV of acceleration voltage, 15 nA of primary current beam, 10 s counting time for each element and 5 s counting time for the background.

Trace element concentrations in minerals have been determined with a LA-ICP-MS housed at IGG-C.N.R., Pavia (Supplementary Material Tab. B) consisting of a PerkinElmer SCIEX ELAN DCR-e quadrupole ICP-MS coupled with a Q-switched Nd:YAG laser source, model Brilliant (Quantel), whose fundamental emission (1064 nm) is converted to 266 nm by two harmonic generators. Spot diameter was typically 50-60 μm. Data reduction was done with the GLITTER software, using the reference synthetic glass NISTSRM 610 as external standard. Si was used as internal standards for zircons, Ca for clinopyroxene. Precision and accuracy were assessed via repeated analysis of BCR-2g reference material, resulting better than ±10% at ppm concentration level. More analytical details are reported in Miller et al. (2012).

In-situ Hf isotopic compositions of zircon have been determined at the State Key Laboratory of Lithospheric Evolution, Institute of Geology and Geophysics of the Chinese Academy of Science (Beijing, China). Zircons were analyzed using a Geolas-193 laser ablation coupled with a Neptune Multi-Collector Inductively Coupled-Plasma Mass-Spectrometer (MC-ICP-MS) as described in Wu et al. (2006). During analyses, isobaric interference of ^{176}Lu on ^{176}Hf was corrected assuming $^{175}Lu/^{176}Lu = 0.02655$; and the isobaric interference of ^{176}Yb on ^{176}Hf was corrected using the average fractionation index measured from the individual analysis proposed by Iizuka and Hirata (2005). Reference zircon 91500 ($^{176}Hf/^{177}Hf = 0.282305$, Wu et al., 2006) was used as a primary

standard for machine calibration, and also Mud Tank was used as a secondary reference material for data evaluation. During analyses, the obtained $^{176}Hf/^{177}Hf$ value from Mud Tank is 0.282521 ± 16 (2SD, n=12), which is consistent with the recommended value of 0.282507 ± 6 (2SD, n=5) within analytical uncertainty (Woodhead and Hergt, 2005). All of the Hf isotopic analyses were performed near the U-Pb spots, and the data are reported in Tab. 2. The calculation of ε_{Hf} and depleted mantle model age (T_{DM}) was done as in Wu et al. (2007).

The O isotope composition of pure separates of orthopyroxene (from MR01CR, FI09C04 and FI09C34 samples), clinopyroxene (FI09C04 and FI09C34 samples) and zircon (only from sample MR01CR) have been analyzed at the I.G.G.-C.N.R., Pisa by conventional laser fluorination (Sharp, 1995) coupled with a Finnigan Delta Plus mass spectrometer. Analyses were performed following methods described by Perinelli et al. (2011). Results are reported in Tab. 3.

Results

U-Pb zircon ages

Separated zircons are anhedral to subhedral, inclusion-free, but locally fractured. Zircons from the Ol-chromitite are slightly pinkish, while those from the Opx-chromitites are colourless. All the separated zircons show low cathodoluminescence (CL). No internal zoning is shown by the Opx-chromitite zircons (Fig. 3) and by most of those from the Ol-chromitite. However, some Ol-chromitite zircons display two different, broad internal domains, the core being slightly darker (Fig. 3). Most of the U-Pb LA-ICP-HRMS analyses of the zircons from Opx-chromitites provide Early Jurassic concordant U-Pb ages. The twenty-nine analyses from twenty-seven FI09C04 zircons provided twenty concordant ages varying from 178 ± 5 to 199 ± 6 Ma (Fig. 4), with a concordia ages of 187 ± 2 Ma (95% confidence level error, MSWD=1.8; Fig. 5). The other single-spots show slightly discordant U-Pb data, but with $^{206}Pb/^{238}U$ ages in the same interval defined by the concordant ages, with exception of zircon 33 showing a Late Triassic age (208 ± 4 Ma; Fig. 4).

Similarly, ten zircon grains from the FI09C34 sample yielded eight concordant ages ranging from 185 ± 6 to 193 ± 7 Ma, with a concordia ages of 187 ± 1 Ma (95% confidence level error, MSWD = 3.2).

Most of the analyses of the MR01CR zircons (twenty-eight out of thirty) also give Lower Jurassic concordant ages ranging mainly from 181 ± 6 to 197 ± 6 Ma and providing a concordia age of 188 ± 1 Ma (95% confidence level error, MSWD = 2.0; Fig. 5). However, the darker internal domain of some zircons provide older ages, two of them giving Triassic (Anisian-Carnian) concordant ages at 242 ± 7 Ma and 229 ± 7 Ma (Tab. 1; Fig. 3, 4).

Major and Trace Mineral chemistry

Chromites from the investigated samples cover the same compositional field defined by those from other FPP chromitite layers documented by Grieco et al. (2001, 2004; Fig. 6). Chromites from the Opx-chromitites also approach the compositions of those from the phlogopite harzburgites-pyroxenites association (Siena and Coltorti, 1989; Zanetti et al., 1999; Grieco et al., 2001), whereas the Ol-chromites from Sasso Rosso show higher Cr#. The same behaviour is shown by the pyroxenes composition, with those from the Opx-chromitites possessing larger Al_2O_3 contents (up to 1.3 wt.%), which approach those in the phlogopite harzburgites-pyroxenites association, while Ol-chromitite pyroxenes have a very Al-poor composition (0.6-0.1 wt.% Al_2O_3). The increase of Al content in pyroxenes is accompanied by a significant decrease of Mg# of pyroxenes and olivine. As a whole, Mg# of pyroxenes and olivines in chromitite layers are distinctly higher than in the phlogopite harzburgites-pyroxenites association.

The clinopyroxene from the Opx-chromitites is strongly enriched in LREE with respect to MREE and HREE (Fig. 7; La_N/Sm_N between 3.09-5.26 and La_N/Yb_N between 21.43-42.47). The REE patterns are comparable with those of the clinopyroxene from the phlogopite harzburgite-pyroxenite association (SIMS analysis: Zanetti et al., 1999), but significantly different from those in late dolomite-apatite-wehrlites and apatite-orthopyroxenites and their host harzburgites (Zanetti et al.,

1999; Morishita et al., 2008). These relationships are also apparent by inspection of the PM-normalised spider diagrams (Primitive Mantle values from McDonough and Sun, 1995), in which the patterns of Opx-chromitite clinopyroxenes match considerably those of the phlogopite harzburgites-pyroxenites association, in particular sharing the very low Nb/LREE ratio, the positive Sr anomaly and the very large Sc/HREE ratio. The trace element concentration of amphibole in sample FI09C34 is strictly similar to those found in the country phlogopite harzburgites, as in the associated clinopyroxenites.

Zircons from Opx-chromitites show very similar trace elements composition. REE patterns are typically HREE-enriched, with La, Pr and Nd between 1-2 xCI (normalized to Chondrite I, CI: Lyubetskaya and Korenaga, 2007), a strong positive Ce anomaly (~10 xCI), and a steady enrichment from Sm to Lu (with maximum at Lu_N from 36 to 53) with a slight negative Eu anomaly (Fig. 8). Th and U concentrations are both ~200 ppm: as a consequence the Th/U is ~1. Pb and Ti are ~6 and ~19 ppm, respectively.

Zircons from Ol-chromitite display REE patterns with the same La and Lu concentration of the Opx-chromitite ones (Fig. 8), but with slightly higher contents from Ce to Yb. Ce and Eu still determine positive and negative anomalies, respectively. Th and U are higher (~480 and ~670 ppm, respectively), with Th/U of ~0.7. Pb and Ti are 7-16 and 7-12 ppm, respectively.

In all the chromitite zircons, HREE and Y are distinctly lower than in the magmatic ones from the External Gabbro (Zanetti et al., 2013) and the nepheline diorite pegmatites (Schaltegger et al., 2015) of the Finero Complex.

Hf and O isotope composition

The zircons from the three studied samples share similar Hf isotopic ratios. In particular, $^{176}Hf/^{177}Hf$ is between 0.282486±18-0.282582±16 and 0.282492±18-0.282587±19 for FI09C04 and FI09C34, respectively, with the weighted average values identical within uncertainty (0.282542±11, MSWD

8.9, 95% conf. for FI09C04; 0.282535±22, MSWD 9.7, 95% conf., for FI09C34). MR01CR zircons have $^{176}Hf/^{177}Hf$ between 0.282550±12-0.282610±13 for, with a weighted average slightly higher thant that the Opx-chromitite zircons (0.282580±8, MSWD 7.9, 95% conf.). The calculated $\varepsilon Hf_{(188)}$ span from -5.9 to -1.6 (Fig. 9), with weighted average values of -3.9 ± 0.4 for FI09C04 (MSWD 7.6, 95% conf.), -4.2 ± 0.8 for FI09C34 (MSWD 9.7, 95% conf.), and -2.7 ± 0.3 for MR01CR (MSWD 7.9, 95% conf.). Badanina et al. (2013), for zircons from FPP chromitite layers reported $^{176}Hf/^{177}Hf$ values similar to those obtained in this study ($^{176}Hf/^{177}Hf$ between 0.282533-0282652 for ~90% of zircons).

Pyroxenes from Opx-Chromitites show very uniform O isotopic compositions, with positive fractionation in orthopyroxene ($\delta^{18}O$ is 6.5-6.7‰ for clinopyroxene, 6.8-6.9‰ for orthopyroxene; Fig. 10). Zircons from Ol-chromitite exhibit comparable $\delta^{18}O$ (6.8‰), but the associated orthopyroxene has significantly lighter O isotopic composition (5.4‰). The $\delta^{18}O$ of the pyroxenes from Opx-chromitites and of the zircons from the Ol-chromitite are significantly higher than the typical range defined by mantle lithologies and mantle-derived melts (5.5-5.9‰ and 5.8-6.2‰, respectively; see Bindeman, 2008 and references therein), as well as of the values reported by Selverstone and Sharp (2011) for a series of lithologies from the FPP, but they more closely match the compositions found in FPP amphiboles and phlogopites by Hartmann and Wedephol (1993).

Discussion

Concepts on the origin of chromitites

Ferrario and Garuti (1990), Garuti et al. (1997), Grieco et al. (2001, 2004), Zaccarini et al. (2004) propose models in which dunites formation and chromitites segregation were linked to the pervasive metasomatism experienced by the FPP, but with significant differences in terms of both series of processes and melt compositions.

In particular, Grieco et al. (2001) proposed that chromite layers and their dunite haloes formed by interaction between basic melts and the ambient harzburgite. The residual melts of this process

336 invaded the country rock harzburgites, with precipitation of clinopyroxene and amphibole. In this
337 scenario, phlogopite crystallisation was a successive event related to the late intrusion of
338 clinopyroxenites, which induced K-metasomatism.
339 Zaccarini et al. (2004) concluded that chromitites and phlogopite metasomatism were the result of
340 the interaction of uprising alkaline-carbonatitic fluids with the ambient harzburgite in the
341 framework of mantle diapirism at the base of the continental crust induced by extensional tectonics.
342 Our data place further constraints on the geochemical affinity of the chromitite parent melts, as well
343 as on its compositional relationships with the metasomatic agent producing the phlogopite-
344 harzburgite and pyroxenite association. The possible effects of the late melt migrations recorded by
345 the FPP have to be evaluated, in particular in terms of zircon and pyroxenes
346 crystallisation/recrystallisation. It has been now widely documented that mantle chromitites after
347 their formation are particularly stable over a very large range of P-T-X conditions, and that they can
348 record the migration of different melts/fluids (Howell et al., 2015), sometimes associated to the
349 precipitation of zircons at mantle depths, over a very large time interval. This issue is relevant for
350 the interpretation of the geochemical evolution of FPP chromitites, because they show some zoning
351 of the mineral chemistry, and variations in the modal content of PGE minerals, which suggest
352 possible interactions with late fluids/melts (Grieco et al., 2001, 2004).
353
354 *Geochemical constraints on chromitites and zircons origin*
355 Several lines of evidence point to a strict geochemical affinity of the parent melts of the chromitite
356 minerals with the metasomatic agents provoking the main metasomatic event of the FPP. First of
357 all, this consideration is supported by the similarity of the major element composition of pyroxenes
358 and spinels (in particular, in terms of very high Mg# and Cr/Al values; Fig. 6) and the evident
359 consistency of the peculiar trace element compositions (i.e. enriched in Th, U and LREE, strongly
360 depleted in HREE) of clinopyroxene and amphibole in the chromitites and in the phlogopite-
361 harzburgites and pyroxenites association (Fig. 7). The similar geochemical affinity of chromitites

and harzburgites and pyroxenites is also supported by the similar trace element fractionation shown by the whole rock data reported by Grieco et al. (2001). The segregation of the chromitite zircons from the same parent melt is suggested by their REE composition. Compared to the magmatic zircons from the external gabbro and nepheline diorite pegmatites, they result enriched in LREE and markedly depleted in HREE, similar to zircons segregated from mantle-derived kimberlites to carbonatites (see Fig. 4 in Hoskin and Schaltegger, 2003). Even more stringent is the match of the peculiar, high $\delta^{18}O$ of the chromitite pyroxenes with those of amphiboles and phlogopites from the phlogopite-harzburgites and pyroxenites association reported by Hartmann and Wedephol (1993). The identical O isotopic composition of MR01CR zircons and Opx-chromitite pyroxenes suggests precipitation from a common parent melt. Although the $\delta^{18}O$ partition coefficent between zircon and mafic phases is presently unconstrained, it has been widely documented that zircons segregated by mantle-derived melts show a very small $\delta^{18}O$ interval at 5.3 ± 0.4 (Valley et al., 2005; Bindeman, 2008; Tribuzio et al., 2014). A further valuable insight into the geochemical signature of the parent melts of the chromitite zircons and on the possible relationships with late melts migrating through the Finero Complex is provided by the zircon $^{176}Hf/^{177}Hf$ ratios, which are much lower than the depleted mantle array. The $\varepsilon Hf_{(188)}$ values are sub-chondritic, at -6.1 ± 0.6 to -1.6 ± 0.5, consistent with the data by Badanina et al. (2013). This observation excludes any genetic relationship with the nepheline diorite pegmatites, whose zircons have $\varepsilon Hf_{(t)}$ between +6 to +9.8, evidence of segregation from mantle-derived melts (Schaltegger et al., 2015).

The melts involved in the pervasive metasomatic event of the FPP, besides having high $\delta^{18}O$ values, were characterised by isotopic composition of Nd, Sr, Pb, H, S, Cl and noble gases indicating the presence of "crustal" components (Hunziker and Zingg, 1982; Voshage et al., 1987, 1988; Cumming et al., 1987; Hartmann and Wedepohl, 1993; Obermiller, 1994; Seitz and Woodland, 2000; Downes, 2001; Matsumoto et al., 2005; Selverstone and Sharp, 2011). The melt migration processes have been mainly attributed to supra-subduction environments (see among others Zanetti

et al., 1999; Grieco et al., 2001, 2004; Morishita et al., 2003, 2008; Matsumoto et al., 2005), but alternatively also to extensional settings (Garuti et al., 2001; Zaccarini et al., 2004).

Negative εHf values are interpreted in the literature as the result of continental crust recycling (e.g. Belusova et al., 2004; Scherer et al., 2007; Lee et al., 2007; Wu et al. 2007). The presence of continental crustal component in the parent melts of chromitite is also strongly supported by the high $\delta^{18}O$ zircon and by the large content in U and Th estimated for the parent melts by clinopyroxene composition and relevant clinopyroxene/liquid partition coefficients, but in particular by the occurrence of thorianite, thorite and uraninite (Zaccarini et al., 2004; this study).

The occurrence of contrasting geochemical signatures in part suggesting oceanic crust derivation (Cumming et al., 1987; Selverstone and Sharp, 2011) may be tentatively interpreted as being related to heterogeneity of the melt source and/or changes in the proportion of melt sources through time.

FPP Chromitite segregation model

Chromitites in dunite bodies are interpreted as late crystallization events of melts migrating into the dunite (Arai and Yurimoto, 1994; Arai, 1997). Such layers are common in dunites from supra-subduction zones, where chromite is basically associated to olivine. The formation of chromitite and surrounding dunite envelope is mainly explained as the result of the interaction between exotic melts and host harzburgite, in association with magma mixing (c.f. Zhou et al., 1994, 1996; Arai, 1997). The reference model assumes that in the first stage, an exotic SiO_2-undersaturated melt, introduced into the ambient peridotite at low pressure, may selectively dissolve pyroxenes, as well as hydrous minerals, and precipitate olivine producing a replacive dunite envelope. This process would form a relatively Si-rich melt, according to the following reaction: SiO_2-poor melt + pyroxenes + hydrous phases → olivine + SiO_2-rich melt. If the dunite channel is further supplied by the SiO_2-undersaturated primary melt, after mixing with the Si-rich melt, an over-saturation in spinel components (Cr+Al) takes place, leading to the isolated precipitation of spinel (c.f. Arai, 1997).

413 Grieco et al. (2001, 2004) proposed that the FPP chromitites and their dunite haloes formed by the
414 interaction between basic melts and the ambient peridotites, where the segregation of phlogopite
415 pyroxenites resulting from successive events of melt migration, unrelated to the chromitites.
416 Instead, Zaccarini et al. (2004) suggested that chromitite layers, dunite channels and phlogopite
417 harzburgites were the result of migration of alkaline-carbonatitic melts.
418 By contrast, Zanetti et al. (1999) stressed that the widespread precipitation of newly-formed,
419 magmatic orthopyroxene in both phlogopite harzburgites and pyroxenites pointed to a SiO_2-
420 saturation of the metasomatic melts related to the pervasive recrystallisation of the FPP. As a
421 consequence, the formation of dunite bodies evidences peculiar variations in melt composition, with
422 pulses of SiO_2-undersaturated melts determining the virtually complete resorption of pyroxenes,
423 amphibole and phlogopite in channels/bodies up to tens of meters across at relatively high, spinel-
424 facies P conditions (see Mazzucchelli et al., 2009). The presence of dunite bodies both concordant
425 to discordant with respect to the mantle foliation, as well as some geochemical changes shown by
426 the magmatic minerals precipitated within dunites indicate that SiO_2-undersaturated melts occurred
427 in different stages of the FPP metasomatic cycle (Giovanardi, 2012).
428 The porphyroclastic textures of the Ol-chromitite MR01CR suggests that the development of
429 structural weaknesses into the dunite bodies may have driven the migration and mixing of the
430 different melt components. The presence of SiO_2-saturated components in the parent melts is
431 confirmed by the nearly ubiquitous presence of newly-formed orthopyroxene replacing olivine. In
432 fact, this feature is present even in the first stages of chromitites formation solely characterised by
433 chromite precipitation (in association to zircon and thorite as accessory mineral phases), as
434 documented by Ol-chromitite MR01CR. The SiO_2-saturation of the melt is more apparent in the
435 Opx-chromitites, which record the complete recovery of the texture characterised by replacement of
436 olivine by secondary orthopyroxene in textural equilibrium with chromite. These petrographic
437 trends, along with the progressive chemical variation from the strongly refractory compositions of
438 the Ol-chromitites to relatively Al-Fe-richer compositions in the Opx-chromitites, allow us to

suggest that the Opx-chromitites are related to levels that experienced the largest time-integrated chromitite melt/dunite ratios.

Two different processes may be envisaged to explain the strong presence of such a metasomatic component in the parent melts of chromitites. The first, according to the Arai's model, is the result of the dissolution of pyroxenes and hydrous minerals of the, already metasomatised, ambient harzburgites-pyroxenites association upon interaction with uprising of mafic melts. This is presumably the general process, always present in any FPP dunite body. However, the occurrence in some dunites of late phlogopite pyroxenites, rich in orthopyroxenes, strictly similar with those forming the main sequence (Grieco et al., 2001; Giovanardi, 2012) suggests that, at least locally, there might be mixing between mafic melts present in dunite channels and new upcoming SiO_2-saturated melts bearing the continental crustal component. The mixing of these two components, at a new transition of the melt composition (i.e. from SiO_2-undersaturated to SiO_2-saturated), may have triggered the precipitation of some chromitites, followed by a segregation of pyroxenites within the dunite bodies.

Interpretation of the U-Pb ages

The age of the petrologic processes recorded by the FPP is still controversial due to a very large time span documented by geochronological investigations, from the Early Permian to the Early Jurassic (Voshage et al., 1987, 1988; Stähle et al., 1990, 2001; Hartmann and Wedephol, 1993; Friedrichsen as cited by Hartmann and Wedephol, 1993; von Quadt et al., 1993; Grieco et al., 2001; Matsumoto et al., 2005; Morishita et al., 2008; Badanina et al., 2013; this work). Apparently late intrusive or metasomatic events (i.e. those documented by Stähle et al., 1990, 2001; the alkaline veins of Grieco et al., 2001; Matsumoto et al., 2005; Morishita et al., 2008) mainly provide Middle Triassic to Early Jurassic ages (from 240 Ma to 195 Ma). The Triassic to Early Jurassic U-Pb ages shown by chromitite zircons can be interpred in two different ways: i) the record of Jurassic,

channelled melt migration with preservation of some Triassic relicts, or ii) the result of the perturbation of the U-Pb zircon systems at Early Jurassic.

The first scenario has some serious drawbacks, among which: 1) the abundance of Triassic to Permian ages of chromitite zircons from the FPP documented by Grieco et al. (2001) (208 ± 2 Ma), Badanina and Malitch (2012) and Badanina et al. (2013) (288 ± 7 Ma; 249 ± 3 Ma; 209 ± 4 Ma); 2) the Triassic age of late alkaline bodies discondatly cutting the harzburgite-pyroxenite association (225 ± 13 Ma; Stähle et al., 2001); 3) the Depleted Mantle geochemical affinity of the intrusives of the associate Finero Mafic Complex showing analogously Triassic to Early Jurassic radiometric data (231 ± 23 Ma to 214 ± 17 Ma: Lu et al., 1997a,b; 232 ± 3 Ma to 214 ± 5 Ma: Zanetti et al., 2013; 212.5 and 190 Ma: Schaltegger et al. 2015). Morever, the petrochemical observations reported in the previous sections clearly indicate that the chromitite zircons were segregated in the early metasomatic cycle producing the phlogopite harzburgites and pyroxenites association of FPP. Thus, it is here proposed that the different age clusters exhibited by the FPP chromitite zircons are the result of progressive re-equilibration stages of the U-Pb system at subsolidus condition.

This is consistent with the absence of CL zoning structures in most of the analyzed zircons of this study showing Early Jurassic ages. It is a common observation for mantle zircons, interpreted as the evidence of compositional homogenization due to a prolonged residence at high temperature in mantle conditions (Corfu et al., 2003).

The re-equilibration of the U-Pb system could most easily have occurred in fluid-assisted conditions. Currently no mineralogical or geochemical data support this hypothesis which, however, cannot be discarded.

In the framework depicted above, the 288 ± 7 Ma age provided by the pinkish zircon population with internal oscillatory-zoning of Badanina et al. (2013) is a minimum age of the FPP pervasive metasomatism. Such an Early Permian age would relate the FPP pervasive metasomatism to the transtensional regime affecting the Variscan orogen, and associated to the formation of the Mafic

Complex of the Val Sesia-Type IVZ, with the emplacement of large volumes of mantle-derived tholeiitic melts at the bottom of the Adria crust (Zanetti et al., 2013 and references therein). The peculiar composition of the metasomatic melts recorded by the FPP requires the concomitant mobilisation of deep-seated reservoirs containing continental crust component. It was possibly related to Variscan subduction of continental crust and metasomatism of the overlying mantle wedge by crustal-derived melts / fluids at ~330 Ma (e.g. Ulten Area, Eastern Alps: Tumiati et al., 2003; Sapienza et al., 2009; Langone et al., 2011).

Evidence for peculiar P-T conditions of the Finero-Type IVZ

According to the reference model of Quick et al. (1995), the mantle bodies of Val Sesia-Type IVZ were already intercalated into the crustal basement at least by the end of the Variscan orogeny, having been progressively incorporated in the cumulates of the underplated Mafic Complex during the Early Permian.

A pronounced re-equilibration of the U-Pb zircon system similar to that shown by chromitite zircons has so far not been documented in the deepest rocks of the Val Sesia-Type IVZ. In particular, although zircons have never been found in associated mantle lithologies, they are common in the gabbroic rocks of the Mafic Complex documenting processes down to 25 km depth (i.e. ~0.8 GPa; Demarchi et al., 1998). Detailed inspections of magmatic zircons from the Mafic Complex performed by Peressini et al. (2007) evidenced the dominant presence of Early Permian ages, with only one Mesozoic age (180 Ma) given by a single-spot on recrystallised “white pest” rim. Consistently, up-to-date reconstructions of the thermal evolution of the polymetamorphic Kinzigite Formation of the IVZ do not provide evidence that the rifting of the Adriatic margin during the Early Jurassic induced conditions capable to reset the U-Pb system in zircon and monazite placed at crustal levels (Handy et al., 1999; Smye and Stockli, 2014; Ewing et al., 2015). Locally, fluid-assisted partial recrystallization of zircon domains at ~220-200 Ma characterises

some IVZ metapelites of the Kinzigite Formation in the transitional zone between Val Sesia-Type IVZ and Finero-Type IVZ (Vavra et al., 1999; Ewing et al., 2013), presumably as a consequence of documented Late Triassic magmatism and of the related fluid activity. Vavra and Schaltegger (1999) also observed that monazites from the Kinzigite Formation yield a subconcordant discordia line with a lower intercept age of 210 ± 14 Ma, interpreted as an episode of fluid-driven Pb loss associated with the influx of hydrothermal fluids.

Thus, it is here speculated that the prolonged re-equilibration of the U-Pb system displayed by chromitite zircons must be associated to peculiar P-T conditions affecting the FPP, such as permanence at great (mantle) depths, possible till the Early Jurassic, and/or a reheating phase due to a later (Early Jurassic) tectono-magmatic activity.

The residence of the FPP at relatively high pressure up to Mesozoic time is supported by the presence of magmatic sapphirine in one of the late, if not the last, magmatic intrusions represented by apatite-calcite-bearing gabbroic dyke swarms, discordantly cutting all the other rocks and structures of the FPP. The precipitation of magmatic sapphirine in gabbroic rocks is consistent with pressures above than 1.1 GPa (Giovanardi et al., 2013). In particular, the composition of sapphirine-saturated melts corresponds to basalt to andesite at pressures of 1.1–1.5 GPa, and the stability field of the magmatic sapphirine extends to P >3 GPa (Milholland and Presnall, 1999). Equilibrium pressures exceeding those at the bottom of the Mafic Complex of the Val Sesia-Type IVZ (i.e. 0.8 GPa), have been also estimated for the Finero Mafic Complex by Siena and Coltorti (1989) at ~1.0 GPa (at ~1000°C). Accordingly, Sills et al. (1983) and Christy (1989) estimated 0.9-1.1 GPa (at T of 800-950°C) for the subsolidus reaction involving formation of metamorphic sapphirine in the gabbroic lithologies of LIZ.

The development of regional thermal positive perturbations in the northern part of the IVZ, possibly associated to asthenosphere upwelling, can be inferred from the Triassic to the Early Jurassic cycles of magmatic activity segregating zircons. This hypothesis is consistent with the high temperature conditions (granulite-facies) argued for the lower IVZ by Brodie and Rutter (1987) in proximity of

541 the Anzola-Val Grande shear zone during the Middle to Late Triassic. It is also indirectly supported
542 by the change of the metamorphic conditions along the Pogallo Line, governed by brittle
543 deformation to the south of Val d'Ossola, and by ductile deformation to the north (Handy, 1987).
544 The temperatures recorded by the cooling paths along the Pogallo Line are consistently higher in
545 the northern than in the southern sector of the IVZ (Wolff et al., 2012).
546
547 *Constraints on the Mesozoic geodynamic evolution of Finero-Type IVZ*
548 Geochronological data supports multiple melt injections throughout the Triassic to Early Jurassic in
549 the Finero-Type IVZ (Zanetti et al., 2013 and references therein). The reappraisal of all data
550 available suggests that a first magmatic stage was dominated by segregation of gabbroic to
551 anorthositic rocks from ~240 to 230 Ma (Gebauer, 1993; Hingerl et al., 2008; Zanetti et al., 2013),
552 possibly associated to the emplacement of anatectic granites in the Kinzigite Formation adjacent to
553 the Finero Complex at 242 ± 3 Ma (Vignola et al., 2008), matching the oldest age found in the core
554 of zircons from MR01CR (242 ± 7 Ma). Volcanic activity also formed (241-238 Ma)
555 porphyroclastic intercalations in the pelagic succession of the western Southern Alps (Mundil et al.,
556 1996). A second main stage was characterised by the intrusion of nepheline diorite pegmatites at
557 225-190 Ma (Klötzli et al., 2007, 2009; Schaltegger et al., 2015). A Late Triassic magmatic event in
558 the FPP is recorded by the emplacement of apatite-carbonate-bearing alkaline diorite and
559 hornblendite dykes at 225-220 Ma and probably also apatite-carbonate-bearing orthopyroxenite
560 veins (240 ± 41 Ma, phlogopite Ar-Ar (Matsumoto et al. 2005) and 213 ± 35 Ma, apatite U-Pb
561 (Morishita et al., 2008).
562 The occurrence of anomalous heating processes at a regional scale has been confirmed by several
563 papers dealing with cooling ages of the IVZ and adjacent area (Wolff et al. 2012; Smye and Stockli,
564 2014; Ewing et al., 2013, 2015; Beltrando et al., 2015). In particular, Beltrando et al. (2015)
565 document the progressive westward rejuvenation of (U-Th)/(He) ages (hereafter ZHe ages), from
566 280-240 Ma in the Lombardian basin to 215-200 Ma near the Sostegno and Fenera basins,

indicating that anomalously high thermal gradients were established in the Late Triassic towards the area where the actual rifting of Alpine Tethys was later localized. This suggests that rift localization along the western margin of the Adriatic plate was probably favoured by a lithospheric thermal anomaly, established at 215-210 Ma, followed by thermal decay at 200-190 Ma (Ewing et al., 2013, 2015; Beltrando et al., 2015).

The Early Jurassic (~200-180 Ma) age interval provided by most of the zircons from the FPP chromitites broadly corresponds to the final stages of extensional faulting as recorded in the IVZ by the Pogallo Line, which was active between 210 and 170 Ma (Zingg et al., 1990), and the Anzola-Val Grande high-T shear zone (Brodie and Rutter, 1987; Brodie et al., 1989), whose movement is considered to have spanned the period between 230-180 Ma. It also matches the final stages of development of the Lombardian Basin at ~220-180 Ma (Bertotti et al., 1999 and references threin), located just east of the IVZ. Although the geodynamic setting of the Middle Triassic deformation stages of the IVZ is still debated (see Zanetti et al., 2013), there is a wide consensus that the Late Triassic-Early Jurassic deformation phases was a precursor events of the opening of the Alpine Tethys, which involved crustal thinning, mantle exhumation and a partial rotation of the IVZ (15° to 23° of tilting; Wolff et al., 2012). It is thus proposed that the age interval shown by colourless smoky chromitite zircons and, in particular, the closure of the U-Pb system of the mantle zircons at ~180 Ma, document the exhumation stage of the FPP.

Smye and Stockli (2014) evidenced that the IVZ underwent a reheating event of sufficient duration and T to reset the U-Pb system of rutile in granulites of the Kinzigite Formation at ~180-190 Ma, possibly due to hyperextension of the Adriatic lithosphere. An Early Jurassic heating has been also invoked to explain the resetting of the ZHe thermochronometer in the Baveno granite (Wolff et al., 2012). Subsequent crust-wide extension led to breakup of continental crust and mantle exhumation. ZHe ages in detrital zircons from syn-tectonic sandstone constrain the onset of normal faulting in the axial zone at 185-180 Ma (Beltrando et al., 2015). It is thus concluded that the ages shown by FPP chromitite zircons record thermal perturbations in the Triassic-Early Jurassic time span, the

youngest one reflecting hyperextension of the Adriatic lithosphere (Smye and Stockli, 2014), and regional Early Jurassic magmatic activity (Mazzucchelli et al., 2010; Schaltegger et al., 2015). The absence of evidence for partial melting in the FPP suggests that such thermal perturbations never exceeded 965°C, which is the solidus temperature extimated for the Finero phlogopite harzburgites (Giovanardi et al., 2013).

Concluding Remarks

Field relationships, the major element composition of spinel and pyroxenes, the trace element composition of clinopyroxene and zircon, the O isotopic composition of zircon and pyroxenes, and the Hf isotopic composition of zircon converge in indicating that the chromitite layers here studied were segregated from hybrid melts derived from the mantle but stronly contaminated by continental crust.

The FPP chromitite zircons yield ages spanning the Early Permian to the Early Jurassic, interpreted as indicating primary crystallization in the Early Permian and resetting during thermal disturbances in the Jurassic. The chromitites zircon data indicate that the FPP was at mantle depths since the Early Permian, being exhumed at shallower, crustal levels only during Early Jurassic. The youngest event appears to have been connected to initiation of continental rifting and mantle exhumation, precursor events of the opening of the Alpine Tethys. Our data, along with those of Grieco et al. (2001), Badanina and Malitch (2012) and Badanina et al. (2013), support that lithosphere rifting and exhumation were affected by two strong thermal perturbations at 208 Ma and 187 Ma.

In our model for the northern IVZ, the pervasive metasomatism of the FPP occurred ~290 Ma and/or before. However, the possibility that the actual age of pervasive metasomatism of FPP was older and related to the Variscan orogenic cycle cannot be excluded.

Acknowledgements

This study is part of the investigations carried out in the frame of the XXV° cycle of PhD degree awarded by the Doctorate School in Science and Technology, University of Pavia.

Tomoaki Morishita, Yumiko Harigane, and Takahito Suzuki are deeply thanked for their assistance during the field work and the samples collection.

We want to thank the two reviewers, Fernando Corfu and Urs Klötzli, for their stimulating and constructive reviews that allowed a significant improvement of the manuscript.

The paper benefited of the Research Support Foundation of the State of São Paulo (FAPESP), in the frame of project 2013/19519-6.

Supplementary Material Captions

Table A: Major-element composition of mineral phases as wt.% and a.p.f.u. Formulae.

Table B: Trace-element compositions of zircons, clinopyroxenes and amphiboles in ppm and single-analysis elements detection limits.

Supplemetary Material C: SEM images and EDS analysis of thorite in sample MR01CR.

References

Arai, S., Yurimoto, H., 1994. Podiform chromitites of the Tari-Misaka ultramafic complex, southwestern Japan, as mantle-melt interaction products. Economic Geology 89(6), 1279-1288.

Arai, S., 1997. Origin of podiform chromitites. Journal of Asian Earth Sciences 15(2–3), 303–310.

Badanina, I.Yu., Malitch, K.N., 2012. Timing of metasomatism in a subcontinental mantle: evidence from zircon at Finero (Italy). Geophysical Research Abstracts 14, EGU2012-7304-1.

Badanina, I.Yu., Malitch, K.N., Belousova, A., 2013. U-Pb and Hf isotope characteristics of zircon from chromitites at Finero. Goldschmidt2013 Conference Abstracts, 639.

642 Belusova, E.A., Griffin, W.L., O'Reilly, S.Y., 2004. Zircon crystal morphology, trace element
643 signature and Hf isotope composition as a tool for petrogenetic modelling: examples from eastern
644 Australia granitoids. Journal of Petrology 47, 329-353.
645 Beltrando, M., Stockli, D.F., Decarlis, A., Manatschal, G., 2015. A crustal-scale view at rift
646 localization along the fossil Adriatic margin of the Alpine Tethys preserved in NW Italy. Tectonics,
647 34/9, 1927-1951.
648 Bertotti, G., Seward, D., Wijbrans, J., Voorde, M.ter, Hurford, A.J., 1999. Crustal thermal regime
649 prior to, during, and after rifting: A geochronological and modeling study of the Mesozoic South
650 Alpine rifted margin. Tectonics 18(2), 185-200.
651 Bindeman, I., 2008. Oxygen Isotopes in Mantle and Crustal Magmas as Revealed by Single Crystal
652 Analysis. Reviews in Mineralogy and Geochemistry 69, 445-478.
653 Blichert-Toft, F., Albarede, F., 1997. The Lu–Hf isotope geochemistry of chondrites and the
654 evolution of the mantle–crust system. Earth Planetary Science Letters 148, 243-258
655 Brodie, K.H., Rutter, E.H., 1987. Deep crustal extensional faulting in the Ivrea Verbano Zone of
656 Northern Italy. Tectonophysics 140, 193-212.
657 Brodie, K.H., Rex, D., Rutter, E.H., 1989. On the age of deep crustal extensional faulting in the
658 Ivrea Zone, Northern Italy. In: Coward, M.P., Dietrich, D., Park, R.G. (Eds), Alpine Tectonics,
659 Geological Society London, Special Publications 45, pp. 203-210.
660 Cawthorn, R.G., 1975. The amphibole peridotite - metagabbro complex, Finero, northern Italy.
661 Journal of Geology 83, 437-454.
662 Christy, A.G., 1989. The stability of sapphirine + clinopyroxene: implications for phase relations in
663 the CaO-MgO-$A1_2O_3$-SiO_2 system under deep-crustal and upper mantle conditions. Contributions
664 to Mineralogy and Petrology 102, 422-428
665 Coltorti, M., Siena, F., 1984. Mantle tectonite and fractionate peridotite at Finero (Italian Western
666 Alps). Neues Jahrbuch für Mineralogie - Abhandlungen 149, 225-244.

667 Corfu, F., Hanchar, J.M., Hoskin, P.W.O., Kinny, P., 2003. Atlas of zircon textures. In: Hanchar,
668 J.M., Hoskin, P.W.O. (Eds.), Zircon. Reviews in Mineralogy and Geochemistry 53, 469-500.
669 Cumming, G.L., Koeppel, V., Ferrario, A., 1987. A lead isotope study of the northeastern Ivrea
670 Zone and the adjoining Ceneri Zone (N Italy): Evidence for a contaminated subcontinental mantle.
671 Contributions to Mineralogy and Petrology 97, 19-30.
672 Demarchi, G., Quick, J.E., Sinigoi, S., Mayer, A., 1998. Pressure gradient and original orientation
673 of a lower-crustal intrusion in the Ivrea^Verbano Zone, Northern Italy. Journal of Geology 106(5),
674 609-622.
675 Downes, H., 2001. Formation and Modification of the Shallow Sub-continental Lithospheric
676 Mantle: a Review of Geochemical Evidence from Ultramafic Xenolith Suites and Tectonically
677 Emplaced Ultramafic Massifs of Western and Central Europe. Journal of Petrology 42 (1), 233-250.
678 Ewing, T.A., Rubatto, D., Hermann, J., 2013. The robustness of the Zr-in rutile and Ti-in-zircon
679 thermometers during high-temperature metamorphism (Ivrea-Verbano Zone, northern Italy).
680 Contribution to Mineralogy and Petrology 165, 757–779.
681 Ewing T.A., Rubatto D., Beltrando·M., Hermann J., 2015. Constraints on the thermal evolution of
682 the Adriatic margin during Jurassic continental break‐up: U–Pb dating of rutile from the Ivrea–
683 Verbano Zone, Italy. Contribution to Mineralogy and Petrology 169, p. 44. DOI 10.1007/s00410-
684 015-1135-6
685 Ferrario, A., Garuti, G., 1990. Platinum-group mineral inclusions in chromitites of the Finero
686 mafic–ultramafic complex (Ivrea-Zone, Italy). Mineralogy and Petrology 41, 125-143.
687 Garuti, G., Oddone, M., Torres, R.J., 1997. Platinum group-element distribution in subcontinental
688 mantle: evidence from the Ivrea Zone (Italy) and the Betic–Rifean Cordillera (Spain and Morocco).
689 Canadian Journal of Earth Sciences 34, 444-463.
690 Gebauer, D., 1993. Pre-Mesozoic geology in the Alps. In: von Raumer, J. F., Neubauer, F. (Eds),
691 The Pre-Alpine evolution of the continental crust of the Central Alps: an overview. Springer-
692 Verlag. pp. 93-117.

693 Giovanardi, T., 2012. Petrological, Geochemical and Geochrnological constraints on the
694 geodynamic evolution of the basic-ultrabasic sequence of Finero (Western Southern Alps).
695 Unpublished PhD Thesis. Department of Earth and Environmental Sciences. pp. 154.
696 Giovanardi, T., Morishita, T., Zanetti, A., Mazzucchelli, M., Vannucci, R., 2013. Igneous
697 sapphirine as a product of melt-peridotite interactions in the Finero Phlogopite-Peridotite Massif,
698 Western Italian Alps. European Journal of Mineralogy 25, 17-31.
699 Giovanardi, T., Mazzucchelli, M., Zanetti A., Langone, A., Tiepolo, M., Cipriani, A., 2014.
700 Occurrence of phlogopite in the Finero Mafic layered complex. Open Geosciences, 6(4), 588–613.
701 Grieco, G., Ferrario, A., von Quadt, A., Köppel, V., Mathez, A., 2001. The zircon-bearing
702 chromitites of the phlogopite peridotite of Finero (Ivrea Zone, Southern Alps): evidence and
703 geochronology of a metasomatized mantle slab. Journal of Petrology 42(1), 89-101.
704 Grieco, G., Ferrario, A., Mathez, E.A., 2004. The effect of metasomatism on the Cr-PGE
705 mineralization in the Finero Complex, Ivrea Zone, Southern Alps. Ore Geology Reviews 24, 299-
706 314.
707 Griffin, W.L., Pearson, N.J., Belousova, E., Jackson, S.E., van Achterbergh, E., O'Reilly, S.Y.,
708 Shee, S.R., 2000. The Hf isotope composition of cratonic mantle: LAM-MC-ICPMS analysis of
709 zircon megacrysts in kimberlites. Geochimica et Cosmochimica Acta 64, 133–147.
710 Handy, M.R., 1987. The structure, age and kinematics of the Pogallo fault zone - Southern Alps,
711 northwestern Italy. Eclogae Geologicae Helvetiae 80, 593–632.
712 Handy, M., Franz, L., Heller, F., Janott, B., Zurbriggen, R., 1999. Multistage accretion, orogenic
713 stacking, and exhumation of continental crust (Ivrea crustal section, Italy and Switzerland).
714 Tectonics 18, 1154-1177.
715 Hartmann, G., Wedepohl, K.H., 1993. The composition of peridotite tectonites from the Ivrea
716 Complex, northern Italy: Residues from melt extraction. Geochimica et Cosmochimica Acta 57,
717 1761-1782.

718 Horstwood, M.S.A., Foster, G.L., Parrish, R.R., Noble, S.R., Nowell, G.L., 2003. Common-Pb
719 corrected in situ U–Pb accessory mineral geochronology by LA-MC-ICP-MS. Journal of Analytical
720 Atomic Spectrometry 18, 837-846.
721 Hoskin, P.W.O., Schaltegger, U., 2003. The composition of zircon and igneous and metamorphic
722 petrogenesis. In: Hanchar, J.M., Hoskin, P.W.O. (Eds), Zircon. Reviews in Mineralogy and
723 Geochemistry 53, 27–62.
724 Hingerl, F., Klötzli, U., Steuber, C., Kleinschrodt, R., 2008. New results from the mafic complex in
725 the Finero area. 33th International Geological Congress, Oslo 6-14th, August 2008, *CD*-ROM
726 abstracts, X-CD Technologies, http://www.cprm.gov.br/33IGC/1344964.html
727 Howell, D., Griffin, W.L., Yang, J.,.Gain, S, Stern, R.A., Huang, J.-X., Jacob, D.E., Xu, X., Stokes,
728 A.J., O'Reilly, S.Y., Pearson, N.J., 2015. Diamonds in ophiolites: Contamination or a new diamond
729 growth environment? Earth and Planetary Science Letters 430, 284–295.
730 Hunziker, J., Zingg, A., 1982. Zur genese der ultrabasischen gesteine der Ivrea-Zone. Schweiz.
731 Mineral. Petr. Mitt. 62, 483-486.
732 Iizuka, T., Hirata, T., 2005. Improvements of precision and accuracy in in-situ Hf isotope
733 microanalysis of zircon using the laser ablation-MC-ICPMS technique. Chemical Geology 220,
734 121-137.
735 Ketchum, J.W.F., Jackson, S.E., Barr, S.M., Culshaw, N.G., 2001. Age, petrochemistry, and
736 tectonic setting of the Paleoproterozoic Lower Aillik Group, Makkovik Province, Canada:
737 evolution of a passive margin – foredeep sequence based on U–Pb (TIMS and LAM-ICP-
738 MS) geochronology. Precambrian Research 105, 331-356.
739 Klötzli, U., Hochleitner, R., Kosler, J., 2007. Lower Triassic mantle-derived magmatism in the
740 Ivrea-Verbano Zone: evidence from laser ablation U-Pb dating of a pegmatite from the eastern
741 Finero Complex (Switzerland). Mitteilungen der Österreichischen Mineralogischen Gesellschaft,
742 153.

743 Klötzli, U., Klötzli, E., Günes, Z., Kosler, J., 2009. Accuracy of Laser Ablation U-Pb Zircon
744 Dating: Results from a Test Using Five Different Reference Zircons. Geostandards and
745 Geoanalytical Research 33(1), 5-15.
746 Langone, A., Braga, R., Massonne, H.J., Tiepolo, M. (2011). Preservation of old (prograde
747 metamorphic) U-Th-Pb ages in unshielded monazite from the high-pressure paragneisses of the
748 Variscan Ulten Zone (Italy). Lithos (DOI: 10.1016/j.lithos.2011.08.007)
749 Langone, A., Tiepolo, M., (2015). U-Th-Pb "multi-phase" approach to the study of crystalline
750 basement: application to the northernmost sector of the Ivrea-Verbano Zone (Alps). Periodico di
751 Mineralogia (2015), 84, 3B (Special issue), xx-xx DOI: 10.2451/2015PM00xx
752 Lee, S.R., Cho, D.L., Cho, M., Wu, F.Y., Kim, H., Jeon, H., 2007. Hf isotopic evidence for
753 Paleoarchean (>3.5 Ga) crustal components in the Korean Peninsula. Geosciences Journal 11, 271-
754 277.
755 Lu, M., Hofmann, A.W., Mazzucchelli, M., Rivalenti, G., 1997a. The mafic-ultramafic complex
756 near Finero (Ivrea-Verbano zone), I. Chemistry of MORB-like magmas. Chemical Geology 140,
757 207-222.
758 Lu, M., Hofmann, A.W., Mazzucchelli, M., Rivalenti, G., 1997b. The mafic-ultramafic complex
759 near Finero (Ivrea-Verbano zone), II. Geochronology and isotope geochemistry. Chemical Geology
760 140, 223-235.
761 Lyubetskaya, T., Korenaga, J., 2007. Chemical composition of Earth's primitive mantle and its
762 variance: 1. Method and results. Journal of Geophysical Research 112, B03211,
763 Ludwig, K.R., 2003. User's manual for ISOPLOT/Ex 3.00, a geochronological toolkit for Microsoft
764 Excel. Berkeley Geochronology Center, Special Publication 4, p. 70.
765 Mundil, R., Brack, P., Meier, M., Rieber, H. and Oberli, F., 1996. High resolution U-Pb dating of
766 Middle Triassic volcanoclastics: Time-scale calibration and verification of tuning parameters for
767 carbonate sedimentation. Earth and Planetary Science Letters 141, 137-151.

768 Mazzucchelli, M., Rivalenti, G., Brunelli, D., Zanetti, A., Boari, E., 2009. Formation of highly
769 refractory dunite by focused percolation of pyroxenite-derived melt in the Balmuccia peridotite
770 massif (Italy). Journal of Petrology 50, 1205-1233.
771 Mazzucchelli, M., Zanetti, A., Rivalenti, G., Vannucci, R., Correia, C.T., Tassinari, C.C.G., 2010.
772 Age and geochemistry of mantle peridotites and diorite dykes from the Baldissero body: Insights
773 into the Paleozoic-Mesozoic evolution of the Southern Alps. Lithos 119, 485-500.
774 Mazzucchelli, M., Quick, J.E., Sinigoi, S., Zanetti, A., Giovanardi, T., 2014. Igneous evolutions
775 across the Ivrea crustal section: the Permian Sesia Magmatic System and the Triassic Finero
776 intrusion and mantle. Goldschmidt Conference – Florence, 2013. Geological field trips, 6(2.2). pp.
777 98. DOI: 10.3301/GFT.2014.05, ISSN: 2038-4947
778 Matsumoto, T., Morishita, T., Masuda, J., Fujioka, T., Takebe, M., Yamamoto, K., Arai, S., 2005.
779 Noble gases in the Finero Phlogopite–Peridotites, ItalianWestern Alps. Earth and Planetary Science
780 Letters 238, 130–145.
781 Miller, C., Zanetti, A., Thöni, M., Konzett, J., Klötzli, U., 2012. Mafic and silica-rich glasses in
782 mantle xenoliths from Wau-en-Namus, Libya: Textural and geochemical evidence for peridotite–
783 melt reactions. Lithos 128-131, 11-26.
784 Milholland, C.S., Presnall, D.C., 1999. Liquidus phase relations in the CaO-MgO-Al_2O_3-SiO_2
785 system at 3.0 GPa: the Aluminous pyroxene thermal divide and high-pressure fractionation of
786 picritic and komatiitic magmas. Journal of Petrology 39, 3–27.
787 Morishita, T., Arai, S., Tamura, A., 2003. Petrology of an apatite-rich layer in the Finero
788 phlogopite–peridotite, Italian Western Alps; implications for evolution of a metasomatising agent.
789 Lithos 69, 37-49.
790 Morishita, T., Hattori, K.H., Terada, K., Matsumoto, T., Yamamoto, K., Takebe, M., Ishida, Y.,
791 Tamura, A., Arai, S., 2008. Geochemistry of apatite-rich layers in the Finero phlogopite–peridotite
792 massif (Italian Western Alps) and ion microprobe dating of apatite. Chemical Geology 251, 99–111.

793 Nowell, G.M., Kempton, P.D., Noble, S.R., Fitton, J.G., Saunders, A.D., Mahoney, J.J., Taylor,
794 R.N., 1998. High precision Hf isotope measurements of MORB and OIB by thermal ionisation
795 mass spectrometry: insights into the depleted mantle. Chemical Geology 149, 211-233.
796 Obermiller, W.A., 1994. Chemical and isotopic variations in the Balmuccia, Baldissero and Finero
797 peridotite massifs (Ivrea-Zone, N-Italy). Unpublished PhD thesis, Johannes Gutenberg-Universität
798 Mainz, pp. 191.
799 Oppizzi, P., Schaltegger, U., 1999. Zircon bearing plagioclasites from the Finero complex (Ivrea
800 zone): dating a Late Triassic mantle hic-cup?. Schweizerische Mineralogische und Petrographische
801 Mitteilungen 79, 330-331.
802 Peressini, G., Quick, J.E., Sinigoi, S., Hofmann, A.W., Fanning, M., 2007. Duration of a Large
803 Mafic Intrusion and Heat Transfer in the Lower Crust: a SHRIMP U/Pb Zircon Study in the Ivrea-
804 Verbano Zone (Western Alps, Italy). Journal of Petrology 48, 1185-1218.
805 Perinelli, C., Armienti, P., Dallai, L., 2011. Thermal Evolution of the Lithosphere in a Rift
806 Environment as Inferred from the Geochemistry of Mantle Cumulates. Northern Victoria Land,
807 Antarctica. Journal of Petrology 52(4), 665-690.
808 Quick, J.E., Sinigoi, S., Mayer, A., 1995. Emplacement of mantle peridotite in the lower continental
809 crust, Ivrea-Verbano Zone, northwest Italy. Geology 23(8), 739-742.
810 Quick, J. E., Sinigoi, S., Peressini G., Demarchi, G., Wooden, J., Sbisà, A., 2009. Magmatic
811 plumbing of a large Permian caldera exposed to a depth of 25 kilometers. Geology 3(7), 603-606.
812 Raffone, N., Le Fèvre, B., Ottolini, L., Vannucci, R., Zanetti, A., 2006. Light-Lithophile Element
813 Metasomatism of Finero Peridotite (W ALPS): A Secondary-Ion Mass Spectrometry Study.
814 Microchimica Acta 155, 251-255.
815 Rivalenti, G., Garuti, G., Rossi, A., Siena, F., Sinigoi, S., 1981. Existence of different peridotite
816 types and of a layered igneous complex in the Ivrea Zone of the Western Alps. Journal of Petrology
817 22, 127-153.

818 Rivalenti, G., Mazzucchelli, M., Vannucci, R., Hofmann, A. W., Ottolini, L., Bottazzi, P. and
819 Obermiller, W., 1995. The relationship between websterite and peridotite in the Balmuccia
820 peridotite massif (NW Italy) as revealed by trace element variations in clinopyroxene. Contributions
821 to Mineralogy and Petrology 121, 275-288.
822 Rivalenti, G., Mazzucchelli M., 2000. Interaction of mantle derived magmas and crust in the Ivrea-
823 Verbano Zone and the Ivrea mantle peridotites. In: Ranalli G., Ricci C.A. and Trommsdorff V.
824 (Eds.). Crust Mantle Interactions, Proceedings of the International School Earth and Planetary
825 Sciences, pp. 153-198.
826 Rutter, E., Brodie, K., James, T., Burlini, L., 2007. Large-scale folding in the upper part of the
827 Ivrea-Verbano zone, NW Italy. Journal of Structural Geology 29, 1-17.
828 Sapienza, G.T., Scambelluri, M., Braga R., 2009. Dolomite-bearing orogenic garnet peridotites
829 fitness fluid-mediated carbon recycling in a mantle wedge (Ulten Zone, Eastern Alps, Italy).
830 Contributions to Mineralogy and Petrology 158, 401–420.
831 Schaltegger U., Ulianov A., Muntener O., Ovtcharova M., Peytcheva I., Vonlanthen P., Vennemann
832 T.W., Antognini M., Girlanda F., 2015. Megacrystic zircon with planar fractures in miaskite-type
833 nepheline pegmatites formed at high pressures in the lower crust (Ivrea Zone, southern Alps,
834 Switzerland). American Mineralogist 100, 83-94.
835 Scherer, E.E., Whitehouse, M.J., Münker, C., 2007. Zircon as a monitor of crustal growth. Elements
836 3(1), 19-24.
837 Seitz, H.M., Woodland, A.B., 2000. The distribution of lithium in peridotitic and pyroxenitic
838 mantle lithologies — an indicator of magmatic and metasomatic processes. Chemical Geology 166,
839 47–64.
840 Selverstone, J., Sharp, Z.D., 2011. Chlorine isotope evidence for multicomponent mantle
841 metasomatism in the Ivrea Zone. Earth and Planetary Science Letters 310, 429-440.

842 Siena, F., Coltorti, M., 1989. The petrogenesis of a hydrated mafic - ultramafic complex and the
843 role of amphibole fractionation at Finero (Italian Western Alps). Neues Jahrbuch für Mineralogie 6,
844 255-274.
845 Sills, Jane D., Ackermand, D., Herd, Richard K., Windley, Brian F., 1983. Bulk composition and
846 mineral parageneses of sapphirirne-bearing rocks along a gabbro-lherzolite contact at Finero, Ivrea
847 Zone, N Italy. Journal of Metamorphic Geology 1, 337-351.
848 Sinigoi, S., Quick, J. E., Mayer, A., Budhan, J., 1996. Influence of stretching and density contrasts
849 on the chemical evolution of continental magmas: an example from the Ivrea-Verbano Zone.
850 Contributions to Mineralogy and Petrology 123, 238-250.
851 Sinigoi, S., Quick, J. E., Demarchi, G., Klötzli, U., 2011. The role of crustal fertility in the
852 generation of large silicic magmatic systems triggered by intrusion of mantle magma in the deep
853 crust. Contribution to Mineralogy and Petrology 162, 691–707.
854 Smye, A.J., Stockli, D.F., 2014. Rutile U–Pb age depth profiling: a continuous record of
855 lithospheric thermal evolution. Earth and Planetary Science Letteers 408, 171–182.
856 Stähle, V., Frenzel, G., Kober, B., Michard, A., Puchelt, H., Schneider, W., 1990. Zircon syenite
857 pegmatites in the Finero peridotite (Ivrea Zone): evidence for a syenite from a mantle source. Earth
858 and Planetary Science Letters 101, 196-205.
859 Stähle, V., Frenzel, G., Hess, J. C., Saupé, F., Schmidt, S. Th., Schneider, W., 2001. Permian
860 metabasalt and Triassic alkaline dykes in the Northern Ivrea Zone: clues to the post-Variscan
861 geodynamic evolution of the Southern Alps. Schweizerische Mineralogische und Petrographische
862 Mitteilungen 81, 1-21.
863 Steck, A., Tièche, J.C., 1976. Carte géologique de l'antiforme péridotitique de Finero avec des
864 observations sur les phases de déformation et de recristallisation. Bulletin Suisse de Minéralogie et
865 de Pétrographie 56, 501-512.
866 Tiepolo, M., 2003. Pb geochronology of zircon with laser ablation inductively coupled plasma-mass
867 spectrometry. Chemical Geology 199, 159-177.

868 Tribuzio, R., Renna, M.R., Dallai, L., Zanetti, A., 2014. The magmatic–hydrothermal transition in
869 the lower oceanic crust: Clues from the Ligurian ophiolites, Italy. Geochimica et Cosmochimica
870 Acta 130, 188-211.
871 Tumiati, S., Thöni M., Nimis P., Martin S., Mair V., 2003. Mantle-crust interactions during
872 Variscan subduction in the Eastern Alps (Nonsberg-Ulten zone): geochronology and new
873 petrological constraints. Earth and Planetary Science Letters 210, 509-526.
874 Van Achterbergh, E., Ryan, C.G., Jackson, S.E., Griffin, W.L., 2001. Data reduction software for
875 LA-ICP-MS: appendix. In: Sylvester, P.J. (Ed.), Laser Ablation-ICP-Mass Spectrometry in the
876 Earth Sciences: Principles and Applications, Mineralog. Assoc. Canada (MAC) Short Course
877 Series, Ottawa, Ontario, Canada, 29, 239-243.
878 Vavra, G., Schmid, R. and Gebauer, D., 1999. Internal morphology, habit and U-Th-Pb
879 microanalysis of amphibolite-to-granulite facies zircons: Geochronology of the Ivrea Zone
880 (Southern Alps). Contributions to Mineralogy and Petrology 134, 380-404.
881 Vavra, G., Schaltegger, U., 1999. Post-granulite facies monazite growth and rejuvenation during
882 Permian to Lower Jurassic thermal and fluid events in the Ivrea Zone (Southern Alps).
883 Contributions to Mineralogy and Petrology 134, 405-414.
884 Vignola, P., Diella V., Oppizzi P., Tiepolo M., Weiss S., 2008. Phosphate assemblages from the
885 Brissago granitic pegmatite, western Southern Alps, Switzerland. The Canadian Mineralogist 46,
886 635-650.
887 von Quadt, A., Ferrario, A., Diella, V., Hansmann, W., Vavra, G., Köppel, V., 1993. U-Pb ages of
888 zircons from chromitites of the phlogopite peridotite of Finero, Ivrea Zone, N-Italy. Schweizerische
889 Mineralogische und Petrographische Mitteilungen 73, 137-138.
890 Voshage, H., Hunziker, J.C., Hofmann, A.W., Zingg, A., 1987. A Nd and Sr isotopic study of the
891 Ivrea zone, Southern Alps, N-Italy. Contributions to Mineralogy and Petrology 97, 31-42.

892 Voshage, H., Sinigoi, S., Mazzucchelli, M., Demarchi, G., Rivalenti, G., Hofmann, A.W., 1988.
893 Isotopic constraints on the origin of ultramafic and mafic dikes in the Balmuccia peridotite
894 (Ivrea Zone). Contributions to Mineralogy and Petrology 100(3), 261-267.
895 Wiedenbeck, M., Alle, P., Corfu, F., Griffin, W.L., Meier, M., Oberli, F., von Quadt, A., Roddick,
896 J.C., Spiegel, W., 1995. Three natural zircon standards for U–Th–Pb, Lu–Hf, trace elements ad
897 REE analyses. Geostandard Newsletter 19, 1-23.
898 Woodhead, J.D., Hergt, J.M., 2005. A preliminary appraisal of seven natural zircon reference
899 materials for in-situ Hf-isotope analysis. Geostandard and Geoanalytical Research 29, 183–195.
900 Wolff, R., Dunkl, I., Kiesselbach, G., Wemmer, K., Siegesmund S., 2012. Zircon (U-Th)/He and
901 fission track constraints on the exhumation history of the Ivrea-Verbano Zone of the Southern Alps.
902 Tectonophysics 579, 104-117.
903 Wu, F.Y., Yang, Y.H., Xie, L.W., Yang, J.H., Xu, P., 2006. Hf isotopic compositions of the
904 standard zircons and baddeleyites used in U–Pb geochronology. Chemical Geology 234, 105-126.
905 Wu, F.-Y., Yang, J.-H., Wilde, S.A., Liu, M.-X., Guo, J.-H., Zhai, M.-G., 2007. Detrital zircon U-
906 Pb and Hf isotopic constrains on the crustal evolution of North Korea. Precambrian Research 159,
907 155−177.
908 Zaccarini, F., Stumpfl, E.F., Garuti, G., 2004. Zirconolite and Zr–Th–U minerals in chromitites of
909 the Finero complex, western Alps, Italy: evidence for carbonatite-type metasomatism in a
910 subcontinental mantle plume. The Canadian Mineralogist 42, 1825-1845.
911 Zanetti, A., Mazzucchelli, M., Rivalenti, G., Vannucci, R., 1999. The Finero phlogopite-peridotite
912 massif: an example of subduction-related metasomatism. Contributions to Mineralogy and
913 Petrology 134, 107-122.
914 Zanetti, A., Mazzucchelli, M., Sinigoi, S., Giovanardi, T., Peressini, G., Fanning, M., 2013.
915 SHRIMP U-Pb ZirconTriassic Intrusion Age of the Finero Mafic Complex (Ivrea-Verbano Zone,
916 Western Alps) and its Geodynamic Implications. Journal of Petrology 54, 2225-2265.

917 Zanetti, A., Mazzucchelli, M., Sinigoi, S., Giovanardi, T., Peressini, G., Fanning, M., 2014.
918 SHRIMP U-Pb Zircon Triassic Intrusion Age of the Finero Mafic Complex (Ivrea-Verbano Zone,
919 Western Alps) and its Geodynamic Implications. Journal of Petrology 55(6), 1239-1240.
920 Zingg, A., Handy, M. R., Hunziker, J. C., Schmid, S.M., 1990. Tectonometamorphic history of the
921 Ivrea Zone and its relationship to the crustal evolution of the Southern Alps. Tectonophysics 182,
922 169-192.
923 Zhou, M.F., Robinson, P.T., Bai, W.J., 1994. Formation of podiform chromitites by melt/rock
924 interaction in the upper mantle. Mineralium Deposita 29(1), 98-101.
925 Zhou, M.-Fu, Robinson, P.T., Malpas, J., Li, Z., 1996. Podiform Chromitites in the Luobusa
926 Ophiolite (Southern Tibet): Implications for Melt-Rock Interaction and Chromite Segregation in the
927 Upper Mantle. Journal of Petrology 37(1), 3-21.
928

929 **Figure Captions**

930 Figure 1 – (a) Sketch map of the Ivrea-Verbano Zone, which represents the westernmost part of the
931 Southern Alps. The rectangle indicates the location of the map of the Finero Complex in (b). CL,
932 Cremosina Line; IL, Insubric Line; CMBL, Cossato-Mergozzo-Brrissago Line; PL, Pogallo Line;
933 HTSZ, high-temperature shear zone of the Anzola-Val Grande area (Brodie and Rutter, 1987;
934 Rivalenti and Mazzucchelli, 2000; Rutter et al., 2007). (b) Sketch map of the Finero Complex
935 modified after Steck and Tièche (1976). The empty stars document the locations of the zircon-
936 bearing chromitites here studied.
937

938 Figure 2 – (a) The thickest layer of the FI09C34 chromitite swarm; (b) Chromitite pocket in sample
939 FI09C34; (c) Texture of MR01CR chromitite, which is characterised by segregation of anhedral
940 large chromite overgrowing a matrix formed by porphyroclastic dunite; (d) Allotriomorphic texture
941 of chromite FI09C04 formed by chromite and orthopyroxene, where rounded olivine relicts rarely

942 occur within large orthopyroxene; (e) Allotriomorphic texture of chromitite FI09C34, with presence
943 of serpentinisation along the grain boundary.
944
945 Figure 3 – Cathodoluminescence images of zircons from FI09C04, FI09C34 and MR01CR.
946 FI09C04 and FI09C34 zircons are virtually free from internal structures, while some of those from
947 MR01CR show broad darker areas, usually returning relatively older ages than the lighter ones.
948 Spot analyses are reported toghether with single-spot concordant ages.
949
950 Figure 4 - Age histogram and relative probability diagram of chromitite zircons of this study.
951 Maximum probability age is reported for each sample.
952
953 Figure 5 - Concordia ages calculated with $^{206}Pb/^{238}U$ and $^{207}Pb/^{235}U$ ratios for chromitite zircons
954 from MR01CR, FI09C34 and FI09C04 samples.
955
956 Figure 6 – Major element mineral chemistry of chromitites of this study. Data from literature are
957 reported for comparison: FPP harzburgite-pyroxenite association (Harz-Py) from Zanetti et al.
958 (1999) (a) and Grieco et al. (2001) (c); average FPP harzburgite (Avg. Harz) from Siena and
959 Coltorti (189) (b); chromitite veins (Chromitite) from Grieco et al. (2001, 2004) (c, d)..
960
961 Figure 7 – (a) CI-normalised (Lyubetskaya and Korenaga, 2007) REE patterns and (b) Pyrolite-
962 normalised (McDonough and Sun, 1995) extended trace element diagrams of clinopyroxenes from
963 FI09C04 and FI09C34 chromitites. Literature data are reported for comparison: amphibole from
964 apatite-bearing wehrlites (Ap-Wehrl Amph) and its host harzburgite (Harz Ap-free Amph) from
965 Morishita et al. (2008) (a); clinopyroxene from the harzburgite-pyroxenite association (Harz-Py
966 Cpx) and apatite-bearing wehrlite (Ap-Wehrl Cpx) from Zanetti et al. (1999) (b); clinopyroxene
967 from harzburgite (Harz Cpx) and chromitite veins (Chromitite Cpx) from Grieco et al. (2001) (c).

968

969 Figure 8 – (a) CI-normalised (Lyubetskaya and Korenaga, 2007) REE patterns and (b) Pyrolite-
970 normalised (McDonough and Sun, 1995) extended trace element diagrams for zircons from the
971 chromitites of this study. Data from zircons from (a) gabbros of the EG (Zanetti et al., 2013) and (b)
972 from alkaline dykes within the Mafic Complex (Schaltegger et al., 2015) are reported for
973 comparison.

974

975 Figure 9 – $\varepsilon Hf_{(t)}$ vs U-Pb age for the zircons from the chromitites of this study. Literature data of
976 (a) zircons from miaskite-type nepheline pegmatites in the Finero Mafic Complex (Schaltegger et
977 al., 2015) and (b) FPP chromitites (Badanina et al., 2013). The Depleted Mantle (DM) evolution
978 line is calculated using the values of present-day $^{176}Hf/^{177}Hf$ ratio of 0.28325 from Nowell et al.,
979 1998, and $^{176}Lu/^{177}Hf$ ratio of 0.0384 from Griffin et al., 2000). CHUR values are from Blichert-
980 Toft and Albarede (1997).

981

982 Figure 10 – Isotopic oxygen composition ($\delta^{18}O$ mineral vs. SMOW‰) of orthopyroxene (Opx) and
983 clinopyroxene (Cpx) separates from FI09C04 and FI09C34 chromitites, and of orthopyroxene and
984 zircon (Zrc) separates from MR01CR. FPP data for minerals (Ol = olivine; Cpx = clinopyroxene;
985 Amph = amphibole; Phl = phlogopite) of the harzburgite-pyroxenite association (Harz-Py) from
986 Hartmann and Wedephol (1993) (a) and Selverstone and Sharp (2011) (b) are reported for
987 comparison, as well as the range of mantle peridotites and mantle-derived melts from Bindeman
988 (2008) (*) and zircon values from a hernblende-gabbro and a hornblendite from the Ligurian
989 ophiolites (Tribuzio et al., 2014) (c).

990

991 **Table Captions**

992 Table 1: summary of ELA-ICP-HRMS U-Pb zircon analysis from chromitite layers from FPP.

993

994 Table 2: summary of MC-ICP-MS *in-situ* Hf isotopic compositions of zircon from FPP.

995

996 Table 3: Isotopic oxygen composition ($\delta^{18}O$ vs. SMOW‰) of mineral separates from the FPP
997 chromitites here studied . Numbers between parenthesis represent the number of replicates of the
998 measurements on different aliquots of the same sample.

999

1000 Fig. 1

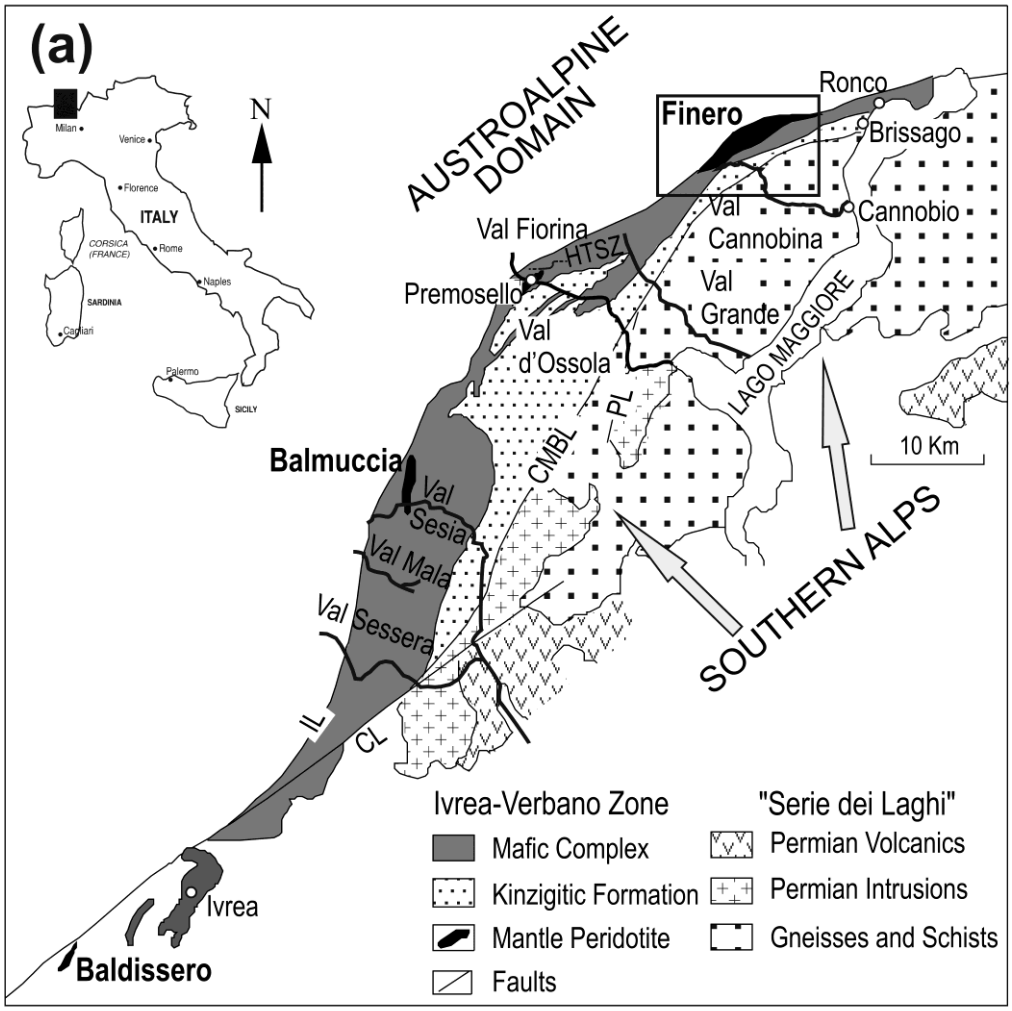

1001

1002

1003 Fig. 2

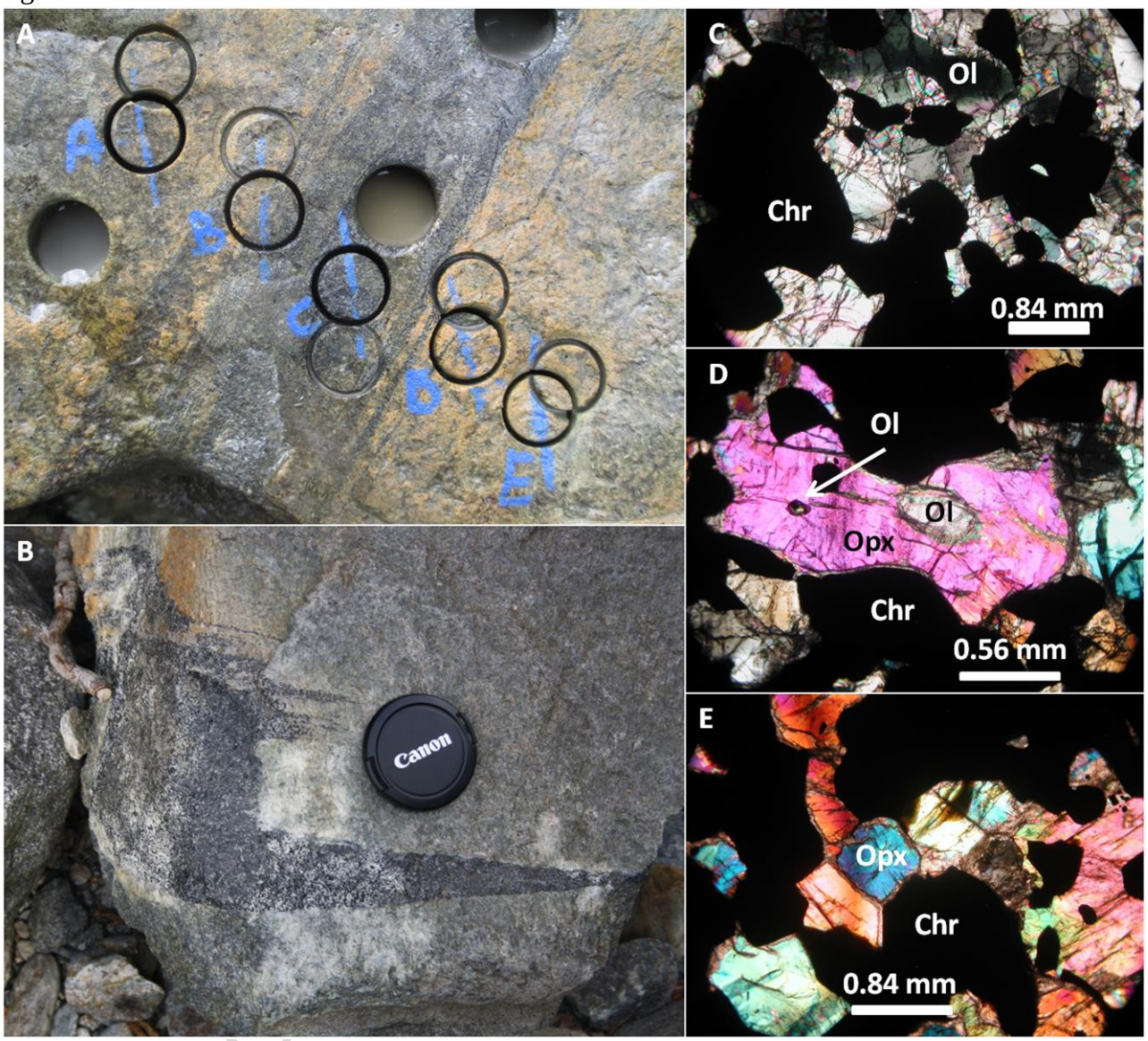

1004

1005

1006 Fig. 3

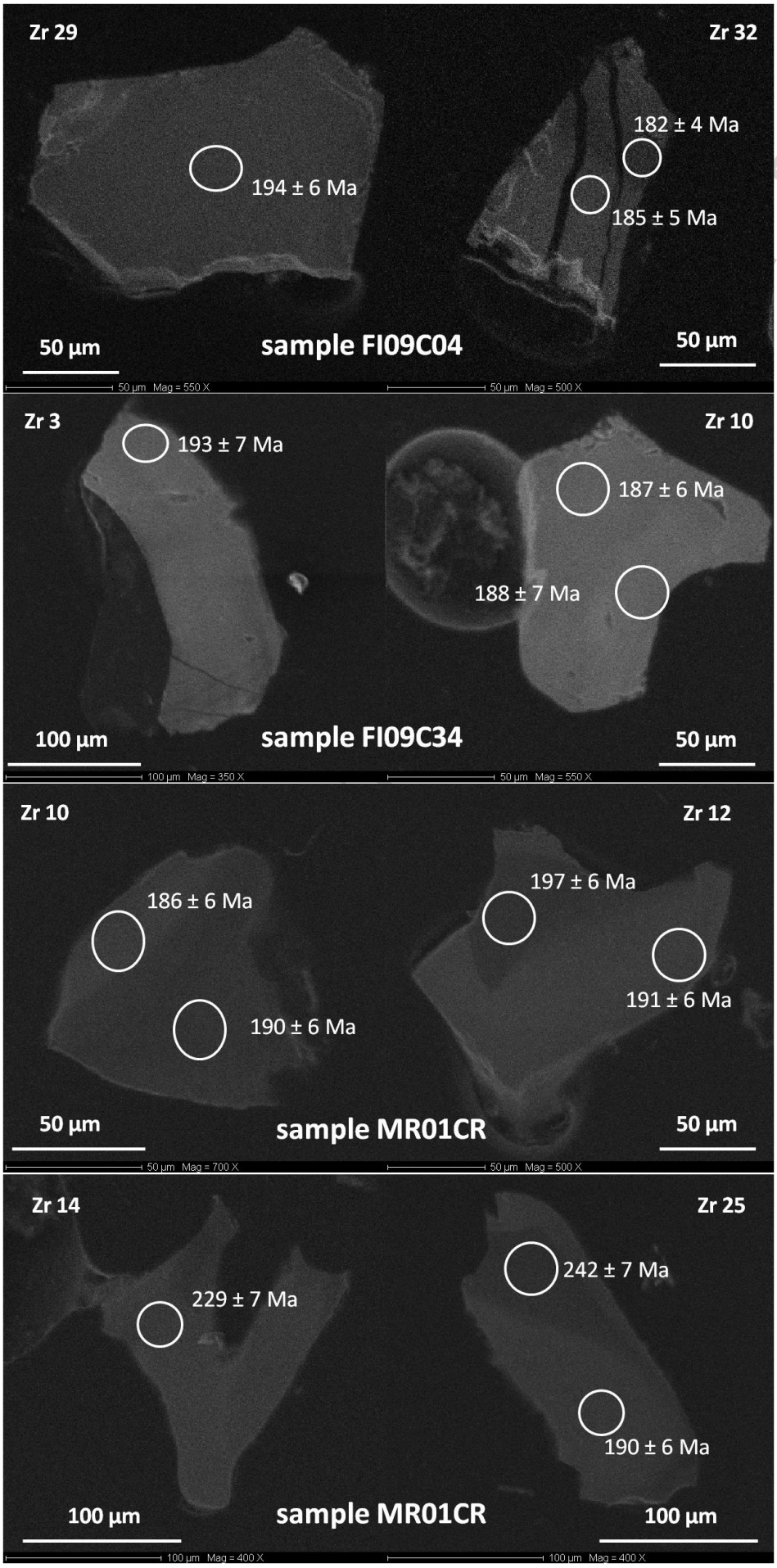

1007

1008

1009 Fig. 4

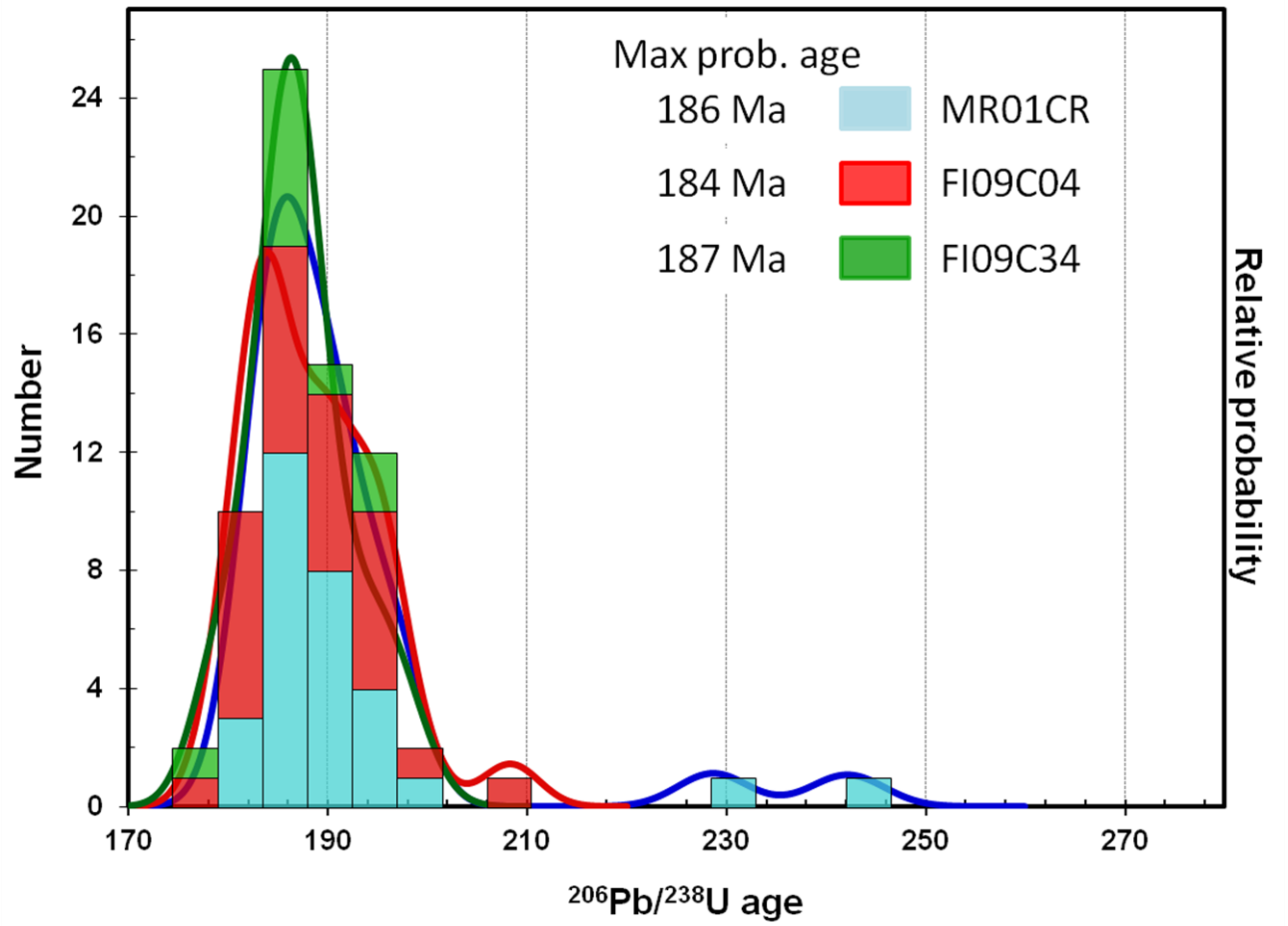

1010

1011

1012 Fig. 5

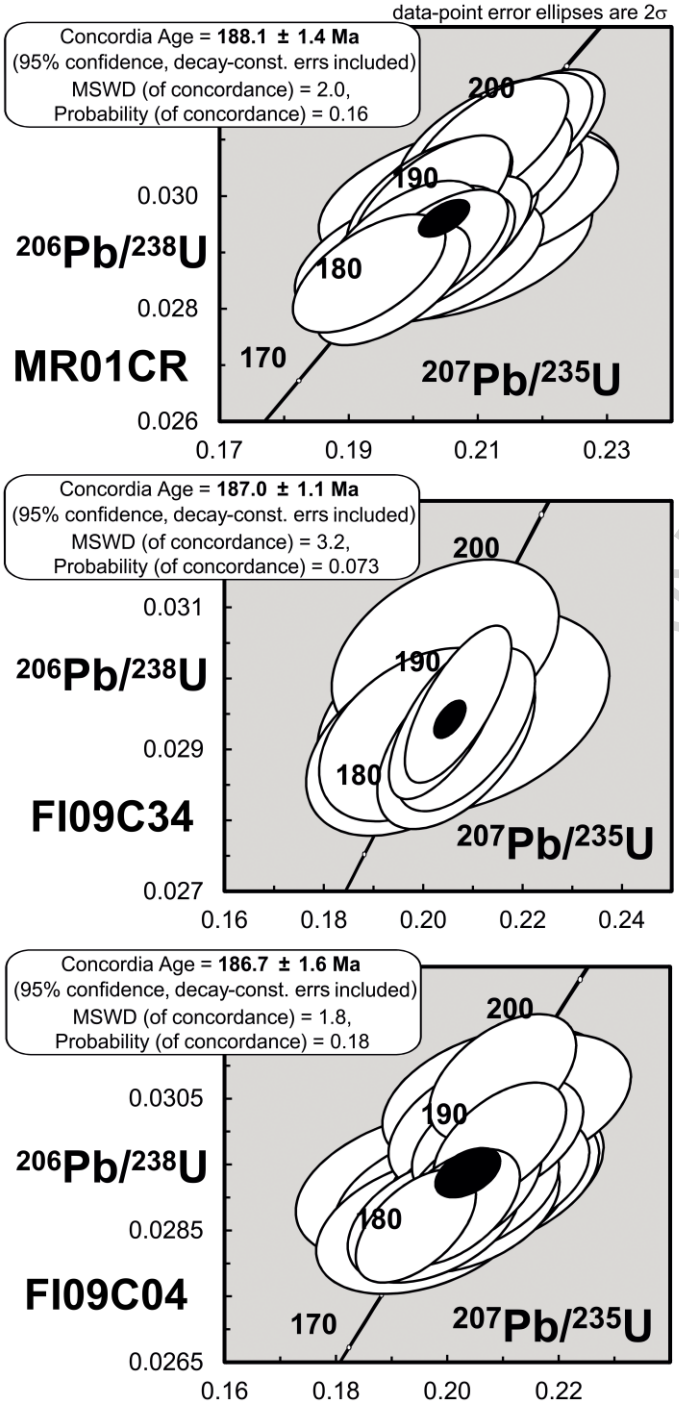

1013

1014

1015 Fig. 6

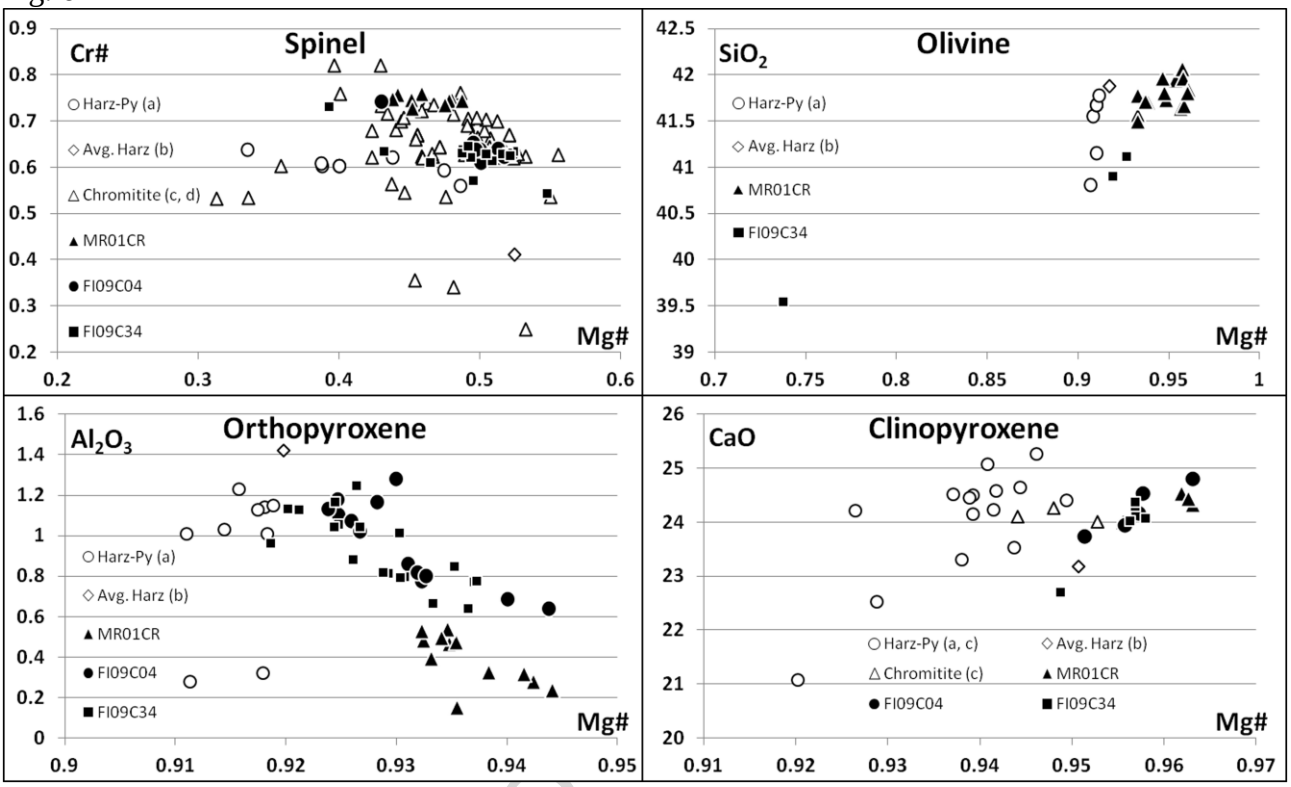

1016

1017

1018 Fig. 7

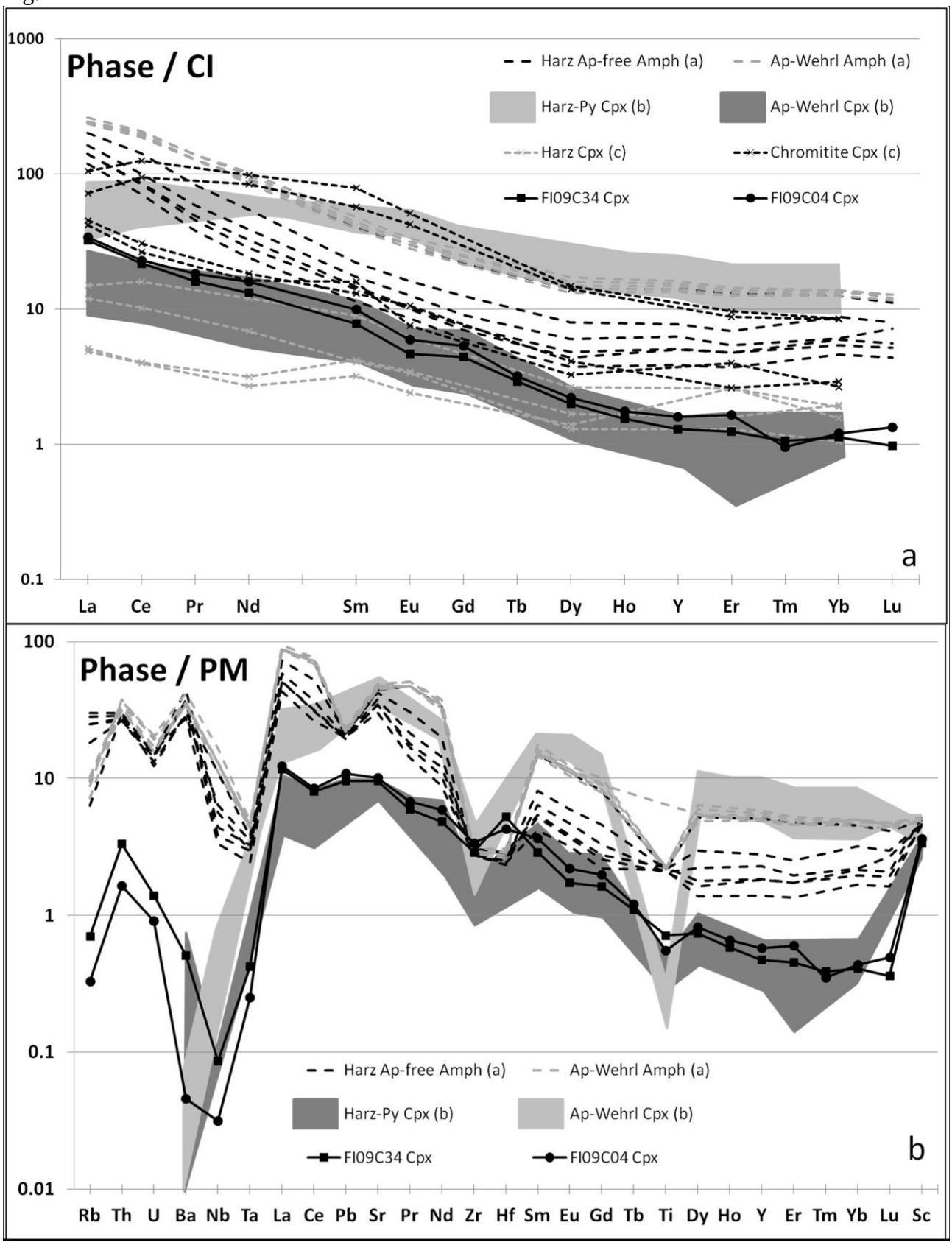

1019

1020

1021 Fig. 8

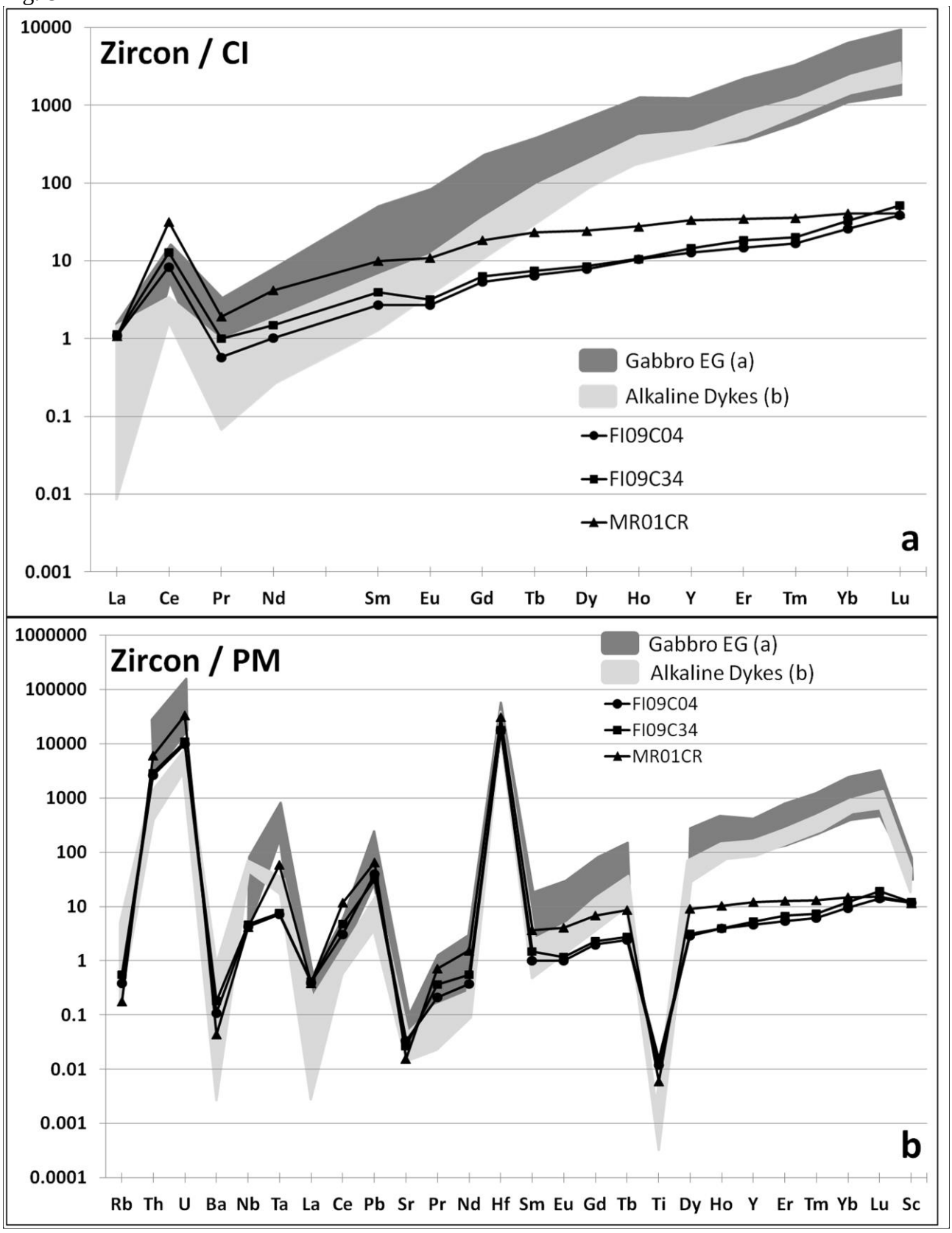

1022

1023

1024 Fig. 9

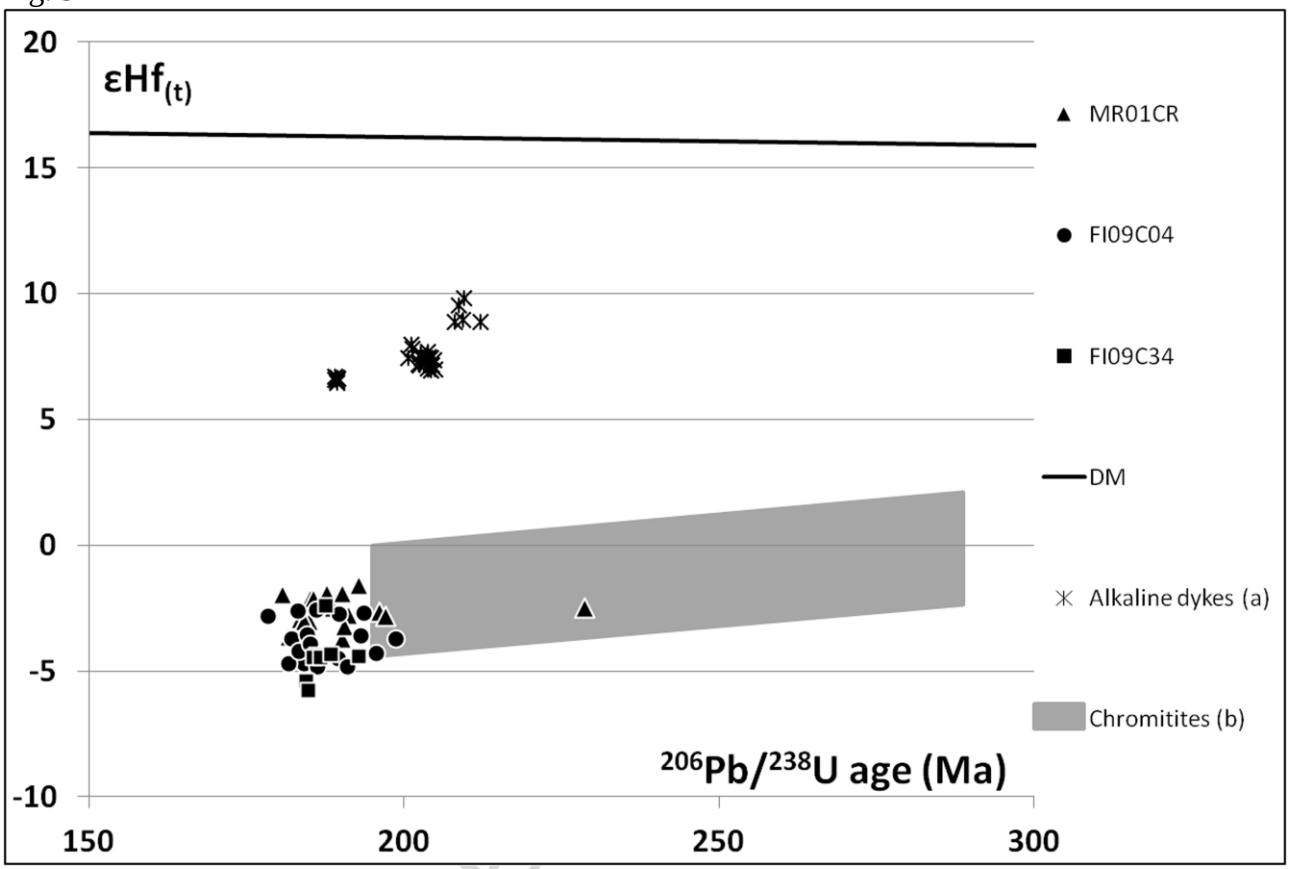

1025

1026

1027 Fig. 10

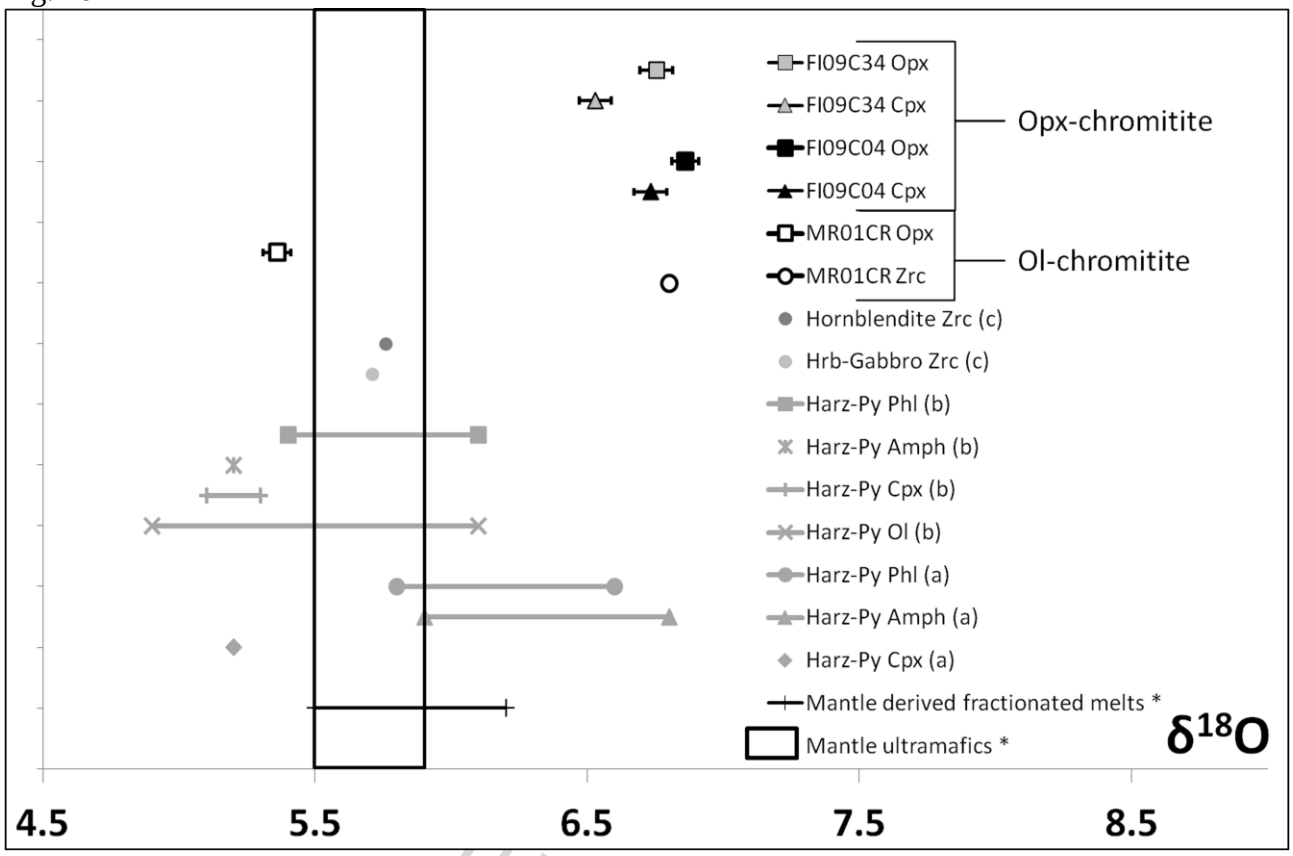

1028

1029

1030 Table 1: summary of ELA-ICP-HRMS U-Pb zircon analysis from chromitite layers from FPP.
1031

Sample: Zircon	MR01 CR Position	Ratio $^{207}Pb/^{206}Pb$	1σ	$^{206}Pb/^{238}U$	1σ	$^{207}Pb/^{235}U$	1σ	Ages $^{207}Pb/^{206}Pb$	2σ	$^{206}Pb/^{238}U$	2σ	$^{207}Pb/^{235}U$	2σ	Concordia	2σ	% of discordance
7	core	0.0498	0.0011	0.0292	0.0005	0.2005	0.0049	187.1	8.3	185.4	5.9	185.6	9.1			
9	core	0.0497	0.0011	0.0309	0.0005	0.2115	0.0051	178.6	7.8	196.2	6.2	194.8	9.4	196.1	6.1	0.69%
9	rim	0.0507	0.0011	0.0290	0.0005	0.2027	0.0049	227.7	9.9	184.3	5.8	187.4	9.0	184.4	5.7	-1.70%
10	core	0.0492	0.0011	0.0299	0.0005	0.2029	0.0050	157.4	7.0	190.0	6.0	187.6	9.2	189.9	6.9	1.31%
10	rim	0.0511	0.0012	0.0292	0.0005	0.2057	0.0051	244.0	11.2	185.7	5.9	189.9	9.5	185.8	5.8	-2.29%
12	core	0.0503	0.0011	0.0310	0.0005	0.2148	0.0053	209.8	9.5	196.9	6.1	197.5	9.7	196.9	6.0	-0.34%
12	rim	0.0511	0.0014	0.0301	0.0005	0.2111	0.0062	245.3	13.5	191.2	6.2	194.4	11.4	191.3	7.1	-1.68%
14	core	0.0509	0.0012	0.0361	0.0006	0.2531	0.0062	238.1	10.8	228.7	7.1	229.1	11.2	228.7	5.0	-0.19%
16	core	0.0494	0.0011	0.0292	0.0005	0.1981	0.0049	165.0	7.6	185.3	5.8	183.5	9.2	185.2	6.7	0.95%
16	rim	0.0516	0.0020	0.0291	0.0005	0.2079	0.0081	269.1	20.4	184.8	6.6	191.8	14.9	184.9	6.5	-3.80%
17	core	0.0506	0.0012	0.0311	0.0005	0.2163	0.0054	222.2	10.2	197.1	6.2	198.9	9.9	197.2	6.1	-0.88%
18	core	0.0498	0.0013	0.0309	0.0005	0.2116	0.0058	186.1	9.6	196.2	6.2	194.9	10.7	196.1	6.1	0.67%
20	core	0.0506	0.0011	0.0304	0.0005	0.2118	0.0052	224.0	10.0	192.8	5.1	195.1	9.6	192.9	5.0	-1.17%
21	core	0.0492	0.0012	0.0299	0.0005	0.2025	0.0052	157.8	7.6	190.0	5.9	187.2	9.7	189.9	5.8	1.48%
23	core	0.0506	0.0015	0.0291	0.0005	0.2018	0.0062	224.0	12.2	185.0	6.0	186.7	10.5	185.1	6.9	-0.88%
24	core	0.0502	0.0012	0.0297	0.0005	0.2054	0.0054	204.3	10.0	188.7	5.1	189.7	11.0	188.7	7.0	-0.56%
25	core	0.0513	0.0011	0.0383	0.0006	0.2697	0.0066	253.0	13.2	242.2	4.6	242.4	8.4	242.2	3.6	-0.11%
25	rim	0.0519	0.0019	0.0299	0.0005	0.2125	0.0078	282.3	14.4	190.1	3.5	195.7	14.4	190.2	3.5	-2.92%
26	core	0.0491	0.0011	0.0286	0.0004	0.1931	0.0048	150.7	7.0	182.0	5.5	179.3	8.9	181.8	4.5	1.48%
27	core	0.0507	0.0014	0.0292	0.0005	0.2038	0.0057	227.7	12.2	185.7	5.8	188.3	11.5	185.7	5.7	-1.43%
28	core	0.0507	0.0012	0.0295	0.0005	0.2055	0.0054	225.8	11.1	187.7	5.9	189.8	10.0	187.8	5.8	-1.14%
28	rim	0.0508	0.0013	0.0295	0.0005	0.2055	0.0057	232.2	11.1	187.2	5.0	189.7	10.5	187.3	5.9	-1.37%
30	core	0.0504	0.0011	0.0284	0.0004	0.1968	0.0049	212.1	9.7	180.7	5.6	182.4	9.0	180.8	5.5	-0.95%
30	rim	0.0499	0.0016	0.0289	0.0005	0.1977	0.0066	188.9	11.1	183.8	5.0	183.1	11.7	183.8	6.9	0.38%
33	core	0.0504	0.0023	0.0300	0.0006	0.2085	0.0095	211.6	11.1	190.4	5.0	192.3	9.4	190.5	5.9	-0.98%
34	core	0.0502	0.0012	0.0291	0.0004	0.2012	0.0051	204.3	9.6	184.9	5.7	186.1	9.4	185.0	6.6	-0.64%
35	core	0.0495	0.0013	0.0300	0.0005	0.2048	0.0057	173.5	9.1	190.4	6.2	189.2	10.5	190.3	6.1	0.61%
35	rim	0.0497	0.0014	0.0301	0.0005	0.2071	0.0062	182.4	10.4	191.4	6.2	191.1	11.4	191.4	5.1	0.14%
38	core	0.0516	0.0015	0.0289	0.0005	0.2047	0.0063	265.9	15.8	183.5	5.8	189.1	11.6	183.6	7.5	-3.08%
39	core	0.0510	0.0012	0.0290	0.0004	0.2031	0.0052	239.9	11.4	184.1	6.6	187.8	9.5	184.2	6.6	-1.99%
Std02123		0.0514	0.0018	0.0466	0.0008	0.3309	0.0016	257.0	17.7	293.5	9.5	290.2	20.3	293.4	9.3	1.10%

1032
1033

Sample: Zircon	FI09C04 Position	Ratio $^{207}Pb/^{206}Pb$	1σ	$^{206}Pb/^{238}U$	1σ	$^{207}Pb/^{235}U$	1σ	Ages $^{207}Pb/^{206}Pb$	2σ	$^{206}Pb/^{238}U$	2σ	$^{207}Pb/^{235}U$	2σ	U-Pb Concordia	2σ	% of discordance
26	core	0.0588	0.0019	0.0297	0.0004	0.2412	0.0078	557.8	35.4	188.9	5.4	219.4	14.2			-16.12%
26	rim	0.0546	0.0011	0.0298	0.0004	0.2243	0.0048	394.6	15.7	189.3	4.6	205.4	8.8			-8.53%
27	core	0.0499	0.0016	0.0287	0.0004	0.1975	0.0063	192.2	12.0	182.2	5.0	183.0	11.7	182.2	4.9	-0.44%
28	core	0.0513	0.0016	0.0288	0.0004	0.2039	0.0066	255.7	16.2	183.2	5.0	188.4	12.2	183.2	4.9	-2.87%
29	core	0.0496	0.0020	0.0305	0.0004	0.2088	0.0084	174.9	14.0	193.7	5.6	192.5	15.5	193.7	5.5	0.62%
30	core	0.0494	0.0012	0.0308	0.0004	0.2099	0.0054	165.9	8.1	195.7	5.0	193.5	9.9	195.6	4.9	1.13%
31	core	0.0482	0.0022	0.0292	0.0005	0.1949	0.0091	110.1	10.3	185.4	5.9	180.8	16.8	185.3	5.8	2.47%
32	core	0.0510	0.0016	0.0291	0.0004	0.2042	0.0065	239.5	14.9	184.7	4.9	188.6	12.0	184.7	4.8	-2.15%
32	rim	0.0493	0.0011	0.0286	0.0004	0.1943	0.0044	162.6	6.9	181.6	5.0	180.3	8.2	181.5	4.4	0.72%
33	core	0.0584	0.0017	0.0328	0.0005	0.2645	0.0080	544.8	32.0	208.3	5.7	238.3	14.4			-14.41%
34	core	0.0509	0.0011	0.0298	0.0004	0.2093	0.0049	235.4	10.4	189.5	4.7	193.0	9.0	189.6	4.7	-1.85%
35	core	0.0586	0.0014	0.0310	0.0004	0.2507	0.0065	553.4	27.4	196.9	5.1	227.2	11.7			-15.39%
36	core	0.0521	0.0012	0.0288	0.0004	0.2070	0.0049	287.6	13.0	183.3	4.5	191.0	9.1			-4.22%
37	core	0.0513	0.0018	0.0293	0.0004	0.2072	0.0074	252.1	17.9	186.0	5.2	191.2	13.7	186.1	5.2	-2.79%
38	core	0.0580	0.0013	0.0308	0.0004	0.2461	0.0058	528.6	23.6	195.4	4.8	223.4	10.5			-14.33%
39	core	0.0672	0.0014	0.0306	0.0004	0.2832	0.0064	842.7	36.1	194.2	4.8	253.2	11.5			-30.40%
40	core	0.0501	0.0022	0.0290	0.0004	0.2008	0.0087	201.5	17.4	184.2	5.7	185.8	16.1	184.2	5.6	-0.88%
41	core	0.0495	0.0020	0.0286	0.0004	0.1957	0.0079	170.6	13.8	181.7	5.4	181.5	14.6	181.7	5.4	0.08%
42	core	0.0509	0.0019	0.0304	0.0004	0.2135	0.0079	234.9	17.3	193.2	5.4	196.5	14.6	193.2	5.4	-1.70%
43	core	0.0592	0.0013	0.0283	0.0004	0.2313	0.0054	573.7	25.4	180.2	4.5	211.3	9.9			-17.27%
44	core	0.0506	0.0012	0.0289	0.0004	0.2011	0.0049	220.4	10.0	183.3	4.6	186.0	9.0	183.4	4.5	-1.45%
46	core	0.0508	0.0015	0.0281	0.0004	0.1969	0.0058	232.7	13.4	178.3	4.8	182.5	10.4	178.4	4.7	-2.32%
47	core	0.0602	0.0014	0.0302	0.0004	0.2508	0.0060	609.7	27.5	191.9	4.9	227.2	11.8			-18.38%
48	core	0.0494	0.0015	0.0301	0.0004	0.2048	0.0063	164.5	9.9	191.2	5.2	189.2	11.6	191.1	5.1	1.04%
50	core	0.0508	0.0015	0.0299	0.0004	0.2089	0.0063	230.4	13.5	189.8	5.0	192.6	11.6	189.8	4.9	-1.50%
51	core	0.0502	0.0024	0.0293	0.0005	0.2045	0.0096	202.4	19.1	186.4	6.1	188.9	17.7	186.4	6.0	-1.34%
52	core	0.0509	0.0012	0.0291	0.0004	0.2042	0.0052	235.4	11.3	185.0	4.8	188.7	9.6	185.1	4.7	-1.96%
53	core	0.0499	0.0021	0.0313	0.0004	0.2150	0.0090	189.4	15.9	198.8	5.7	197.7	16.5	198.8	6.5	0.54%
54	core	0.0510	0.0022	0.0293	0.0005	0.2056	0.0088	240.4	20.6	185.9	5.9	189.9	16.3	185.9	5.8	-2.15%
Std02123		0.05295	0.0022	0.04717	0.0007	0.34439	0.0143	326.7	27.2	297.1	8.9	300.5	25.0	297.2	8.7	-1.10%

Table 1: continue.

1039
1040

Sample:	FI09C34			Ratio						Ages				U-P
Zircon	Position	$^{207}Pb/^{206}Pb$	1σ	$^{206}Pb/^{238}U$	1σ	$^{207}Pb/^{235}U$	1σ	$^{207}Pb/^{206}Pb$	2σ	$^{206}Pb/^{238}U$	2σ	$^{207}Pb/^{235}U$	2σ	Concordi
1	core	0.0494	0.0022	0.0290	0.0005	0.1977	0.0087	166.9	15.2	184.5	6.5	183.2	16.2	184.
2	core	0.0517	0.0015	0.0293	0.0005	0.2084	0.0057	270.8	15.5	186.0	6.0	192.2	10.6	186.
3	core	0.0488	0.0023	0.0304	0.0005	0.2044	0.0093	138.2	13.1	192.9	6.7	188.8	17.2	192.
4	core	0.0492	0.0021	0.0292	0.0005	0.1987	0.0080	157.4	13.2	185.6	6.3	184.0	14.9	185.
5	core	0.0516	0.0017	0.0291	0.0005	0.2066	0.0065	266.4	17.3	184.8	6.2	190.7	12.0	184.
6	core	0.0599	0.0017	0.0270	0.0005	0.2230	0.0062							
6	rim	0.0564	0.0014	0.0282	0.0004	0.2185	0.0052	466.6	23.1	179.0	5.6	200.7	9.5	
7	core	3.8182	3.0059	0.0285	0.0228	15.0262	2.7782							
8	core	0.0569	0.0019	0.0310	0.0005	0.2424	0.0078	486.5	32.7	196.7	6.5	220.4	14.2	
10	core	0.0504	0.0012	0.0294	0.0004	0.2042	0.0046	213.0	10.0	186.7	5.6	188.7	8.4	186.
10	rim	0.0513	0.0030	0.0295	0.0006	0.2080	0.0120	252.1	30.0	187.5	7.6	191.9	22.1	187.
11	core	0.0506	0.0011	0.0296	0.0005	0.2070	0.0044	224.5	10.1	188.3	5.8	191.0	8.1	188.
Std02123		0.0530	0.0021	0.0464	0.0008	0.3388	0.0128	329.2	25.9	292.1	9.9	296.3	22.4	292.

1041 Table 1: continue.
1042

1043 Table 2: summary of MC-ICP-MS *in-situ* Hf isotopic compositions of zircon from FPP.
1044

sample	zircon	position	Age (Ma)	$^{176}Yb/^{177}Hf$	2σ	$^{176}Lu/^{177}Hf$	2σ	$^{176}Hf/^{177}Hf$	2σ	$e_{Hf}(0)$	$e_{Hf}(t)$	2σ	T_{DM}	T_{DM}^{C}	$f_{Lu/Hf}$
MR01CR	9	core	188	0.001629	0.000039	0.000052	0.000001	0.282580	0.000015	-6.77	-2.65	0.53	927	1395	-1.00
MR01CR	10	core	188	0.000730	0.000003	0.000022	0.000000	0.282582	0.000012	-6.73	-2.60	0.44	925	1391	-1.00
MR01CR	12	rim	188	0.000479	0.000008	0.000015	0.000000	0.282577	0.000012	-6.89	-2.77	0.44	931	1402	-1.00
MR01CR	14	core	188	0.000533	0.000025	0.000017	0.000001	0.282584	0.000012	-6.64	-2.51	0.44	921	1386	-1.00
MR01CR	16	core	188	0.000603	0.000010	0.000017	0.000000	0.282596	0.000013	-6.24	-2.11	0.45	906	1360	-1.00
MR01CR	17	core	188	0.000620	0.000019	0.000017	0.000000	0.282575	0.000011	-6.96	-2.83	0.40	933	1406	-1.00
MR01CR	20	core	188	0.000661	0.000007	0.000019	0.000000	0.282610	0.000013	-5.73	-1.60	0.47	886	1328	-1.00
MR01CR	21	core	188	0.000742	0.000012	0.000024	0.000000	0.282600	0.000011	-6.09	-1.97	0.39	900	1351	-1.00
MR01CR	23	core	188	0.000550	0.000025	0.000017	0.000000	0.282553	0.000011	-7.74	-3.61	0.40	964	1455	-1.00
MR01CR	24	core	188	0.000573	0.000004	0.000017	0.000000	0.282585	0.000013	-6.61	-2.48	0.47	920	1384	-1.00
MR01CR	25	rim	188	0.000420	0.000006	0.000013	0.000000	0.282550	0.000012	-7.85	-3.73	0.41	968	1462	-1.00
MR01CR	26	core	188	0.000534	0.000006	0.000016	0.000000	0.282552	0.000013	-7.79	-3.66	0.45	966	1458	-1.00
MR01CR	27	core	188	0.000836	0.000026	0.000025	0.000001	0.282595	0.000012	-6.25	-2.12	0.41	906	1361	-1.00
MR01CR	28	core	188	0.000461	0.000007	0.000013	0.000000	0.282601	0.000013	-6.05	-1.92	0.48	898	1348	-1.00
MR01CR	30	core	188	0.000492	0.000005	0.000014	0.000000	0.282599	0.000013	-6.11	-1.98	0.47	900	1352	-1.00
MR01CR	30	rim	188	0.000990	0.000012	0.000033	0.000000	0.282556	0.000020	-7.63	-3.51	0.72	960	1449	-1.00
MR01CR	33	core	188	0.000382	0.000015	0.000012	0.000000	0.282564	0.000013	-7.34	-3.22	0.47	948	1430	-1.00
MR01CR	34	core	188	0.000404	0.000011	0.000012	0.000000	0.282570	0.000014	-7.15	-3.03	0.48	941	1418	-1.00
MR01CR	35	core	188	0.000783	0.000007	0.000024	0.000000	0.282601	0.000015	-6.05	-1.92	0.54	898	1349	-1.00
MR01CR	38	core	188	0.000403	0.000020	0.000013	0.000000	0.282572	0.000012	-7.06	-2.93	0.44	937	1412	-1.00
MR01CR	39	core	188	0.000409	0.000004	0.000012	0.000000	0.282570	0.000015	-7.16	-3.03	0.53	941	1418	-1.00
FI09C04	26	core	188	0.000531	0.000005	0.000021	0.000000	0.282527	0.000019	-8.68	-4.55	0.66	1000	1515	-1.00
FI09C04	26	rim	188	0.000872	0.000019	0.000033	0.000001	0.282566	0.000016	-7.27	-3.15	0.55	946	1426	-1.00
FI09C04	27	core	188	0.000569	0.000005	0.000022	0.000000	0.282550	0.000016	-7.85	-3.72	0.55	968	1462	-1.00
FI09C04	28	core	188	0.000576	0.000024	0.000024	0.000001	0.282582	0.000016	-6.74	-2.61	0.58	925	1392	-1.00
FI09C04	29	core	188	0.000577	0.000005	0.000022	0.000000	0.282579	0.000016	-6.82	-2.70	0.55	928	1397	-1.00
FI09C04	30	core	188	0.000442	0.000007	0.000017	0.000000	0.282534	0.000016	-8.41	-4.28	0.57	990	1498	-1.00
FI09C04	31	core	188	0.001212	0.000037	0.000047	0.000001	0.282523	0.000019	-8.81	-4.69	0.66	1006	1524	-1.00
FI09C04	32	core	188	0.000572	0.000009	0.000022	0.000000	0.282554	0.000020	-7.71	-3.58	0.70	963	1454	-1.00
FI09C04	33	core	188	0.000638	0.000009	0.000025	0.000000	0.282546	0.000018	-7.99	-3.86	0.65	973	1471	-1.00
FI09C04	34	core	188	0.000613	0.000007	0.000024	0.000000	0.282528	0.000017	-8.63	-4.51	0.58	998	1512	-1.00
FI09C04	35	core	188	0.000626	0.000008	0.000025	0.000000	0.282528	0.000021	-8.64	-4.52	0.73	999	1513	-1.00
FI09C04	36	core	188	0.000754	0.000009	0.000028	0.000000	0.282489	0.000019	-10.00	-5.88	0.66	1052	1599	-1.00

FI09C04	37	core	188	0.000605	0.000011	0.000025	0.000000	0.282582	0.000021	-6.71	-2.59	0.75	924	1391	-1.00
FI09C04	38	core	188	0.000544	0.000011	0.000021	0.000000	0.282486	0.000018	-10.13	-6.01	0.64	1056	1607	-1.00
FI09C04	39	core	188	0.000619	0.000011	0.000026	0.000000	0.282524	0.000021	-8.76	-4.64	0.74	1003	1520	-1.00

1045

sample	zircon	position	Age (Ma)	$^{176}Yb/^{177}Hf$	2σ	$^{176}Lu/^{177}Hf$	2σ	$^{176}Hf/^{177}Hf$	2σ	$e_{Hf}(0)$	$e_{Hf}(t)$	2σ	T_{DM}	T_{DM}^{c}	$f_{Lu/Hf}$
FI09C04	40	core	188	0.000497	0.000018	0.000020	0.000001	0.282522	0.000023	-8.84	-4.71	0.80	1006	1525	-1.00
FI09C04	41	core	188	0.000628	0.000008	0.000024	0.000000	0.282522	0.000022	-8.84	-4.72	0.79	1007	1525	-1.00
FI09C04	42	core	188	0.000493	0.000006	0.000020	0.000000	0.282553	0.000016	-7.73	-3.61	0.57	963	1455	-1.00
FI09C04	44	core	188	0.000690	0.000012	0.000025	0.000000	0.282536	0.000017	-8.36	-4.23	0.59	988	1495	-1.00
FI09C04	46	core	188	0.000976	0.000018	0.000037	0.000000	0.282576	0.000018	-6.94	-2.81	0.64	933	1405	-1.00
FI09C04	48	core	188	0.000558	0.000009	0.000022	0.000000	0.282518	0.000018	-8.97	-4.85	0.65	1012	1534	-1.00
FI09C04	50	core	188	0.000510	0.000018	0.000022	0.000001	0.282578	0.000017	-6.86	-2.74	0.62	930	1400	-1.00
FI09C04	51	core	188	0.000901	0.000005	0.000035	0.000000	0.282519	0.000017	-8.96	-4.84	0.61	1011	1533	-1.00
FI09C04	52	core	188	0.001005	0.000035	0.000041	0.000001	0.282544	0.000019	-8.05	-3.93	0.68	976	1476	-1.00
FI09C04	53	core	188	0.000646	0.000010	0.000026	0.000000	0.282550	0.000018	-7.84	-3.72	0.65	968	1462	-1.00
FI09C34	1	core	188	0.000808	0.000017	0.000031	0.000000	0.282503	0.000020	-9.52	-5.40	0.69	1033	1569	-1.00
FI09C34	2	core	188	0.000783	0.000020	0.000032	0.000001	0.282532	0.000019	-8.50	-4.38	0.69	994	1504	-1.00
FI09C34	3	core	188	0.000886	0.000049	0.000038	0.000002	0.282530	0.000022	-8.55	-4.43	0.76	996	1508	-1.00
FI09C34	4	core	188	0.000575	0.000014	0.000023	0.000000	0.282529	0.000018	-8.58	-4.45	0.64	996	1509	-1.00
FI09C34	5	core	188	0.000646	0.000012	0.000028	0.000000	0.282492	0.000018	-9.90	-5.78	0.63	1048	1593	-1.00
FI09C34	6	rim	188	0.000925	0.000036	0.000039	0.000001	0.282551	0.000032	-7.80	-3.68	1.13	967	1460	-1.00
FI09C34	8	core	188	0.000498	0.000004	0.000019	0.000000	0.282577	0.000018	-6.90	-2.78	0.62	931	1402	-1.00
FI09C34	10	core	188	0.000427	0.000008	0.000018	0.000000	0.282529	0.000020	-8.59	-4.46	0.72	997	1509	-1.00
FI09C34	10	rim	188	0.000651	0.000007	0.000029	0.000000	0.282587	0.000019	-6.55	-2.43	0.69	918	1381	-1.00
FI09C34	11	core	188	0.000881	0.000017	0.000039	0.000000	0.282533	0.000017	-8.46	-4.34	0.59	992	1502	-1.00

1046 Table 2: continue.

1047

Table 3: Isotopic oxygen composition ($\delta_{18}O$ vs. SMOW‰) of mineral separates from the FPP chromitites here studied . Numbers between parenthesis represent the number of replicates of the measurements on different aliquots of the same sample.

Sample	Phase	$\delta^{18}O$ avg.	Std. Dev.
MR01CR	Zrc (1)	6.80	
	Opx (2)	5.36	0.05
FI09C04	Opx (2)	6.86	0.05
	Cpx (3)	6.73	0.06
FI09C34	Opx (2)	6.76	0.06
	Cpx (2)	6.53	0.06

Highlights:

- zircon-bearing mantle chromitites formed along with the Finero phlogopite harzbugites
- the Finero Phlogopite Peridotite was firstly metasomatised in Early Permian or before
- younger ages record thermal perturbations related to tectono-magmatic events
- the exhumation of Finero Phlogopite Peridotite occurred in Early Jurassic
- the IVZ exhumation was accompanied by a thermal perturbation at ~187 Ma